A continuum mechanics model of enzyme-based tissue degradation in cancer therapies

Manon Deville, Roberto Natalini, Clair Poignard

A continuum mechanics model of enzyme-based tissue degradation in cancer therapies

Manon Deville, Roberto Natalini, Clair Poignard

RESEARCH REPORT
N° 9030
February 2017
Project-Teams Monc

ISSN 0249-6399 ISRN INRIA/RR--9030--FR+ENG

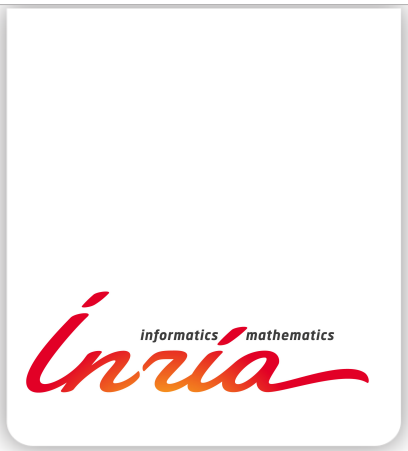

A continuum mechanics model of enzyme-based tissue degradation in cancer therapies

Manon Deville, Roberto Natalini, Clair Poignard *

Project-Teams Monc

Research Report n° 9030 — February 2017 — 42 pages

Abstract: We propose a mathematical model to describe enzyme-based tissue degradation in cancer therapies. The proposed model combines the poroelastic theory of mixtures with the transport of enzymes or drugs in the extracellular space. The effect of the matrix degrading enzymes on both the tissue's composition and its mechanical response is included in the model. Numerical simulations in 1D, 2D and axisymmetric (3D) configurations show how an injection of matrix degrading enzymes alters the porosity of a biological tissue. We eventually exhibit the main consequences of a matrix degrading enzyme pretreatment in the framework of chemotherapy: the removal of the diffusive hindrance to the penetration of therapeutic molecules in tumors and the reduction of interstitial fluid pressure which improves transcapillary transport. Both effects are consistent with previous biological data.

Key-words: Mathematical biology, Poroelasticity, ECM degradation, Interstitial fluid pressure, Tissue distribution

INRIA Bordeaux-Sud-Ouest, CNRS UMR 5251

Université de Bordeaux, 351 cours de la Libération, 33405 Talence Cedex, France

Istituto per le Applicazioni del Calcolo "M. Picone", Consiglio Nazionale delle Ricerche, Via dei Taurini 19, I-00185 Rome, Italy

* Corresponding author : clair.poignard@inria.fr

RESEARCH CENTRE
BORDEAUX – SUD-OUEST

200 avenue de la Vieille Tour
33405 Talence Cedex

Un modèle basé sur la mécanique des milieux continus pour la dégradation tissulaire par traitement enzymatique dans les thérapies contre le cancer

Résumé : On propose un modèle pour décrire la dégradation tissulaire par traitement enzymatique dans les thérapies contre le cancer. Le modèle proposé combine la théorie des mélanges en poroélasticité avec le transport des enzymes ou des médicaments dans l'espace extracellulaire. L'effet des enzymes qui dégradent la matrice extracellulaire sur à la fois la composition du tissu et sa réponse mécanique est inclu dans le modèle. Les simulations numériques dans des configurations 1D, 2D et en axisymétrie (3D) montrent comment une injection d'enzymes dégradant la matrice extracellulaire altère la porosité d'un tissu biologique. On met en évidence à terme les conséquences principales d'un traitement enzymatique dans les thérapies contre le cancer : l'élimination de l'obstacle à la pénétration par diffusion de molécules thérapeutiques dans les tumeurs et la réduction de la pression interstitielle, améliorant ainsi le transport transcapillaire. Ces deux effets sont en accord avec des données biologiques existantes.

Mots-clés : Biologie mathématique, Poroélasticité, Dégradation de la matrice extracellulaire, Pression interstitielle, Distribution tissulaire

Contents

1 Introduction

1.1 Motivations

The use of macromolecules as therapeutic agents has come to the forefront in cancer research in recent years. But macromolecular-based therapies are challenging, particularly those involving intracellular targets. Indeed, one needs to consider the multiple biological barriers that stand between the drug at its site of administration and its ultimate biological target [42, 31].

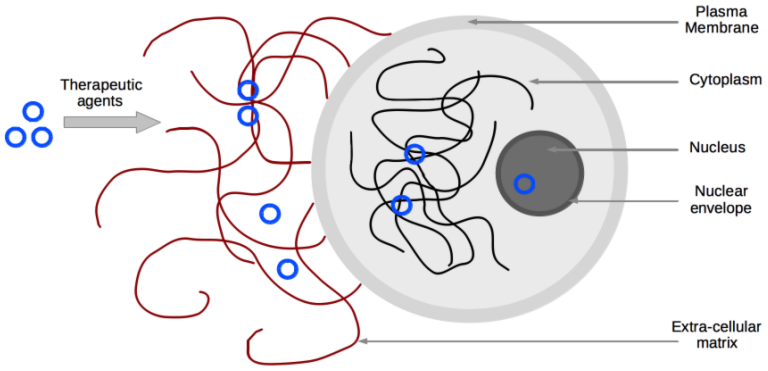

Figure 1: After its injection into the target tissue, a therapeutic agent encounters biological barriers from extracellular environment toward the interior of the target cell.

Transport through the extracellular matrix (ECM) is a critical step in cell targeted drug delivery. To reach the cell membrane, the therapeutic agent must diffuse through the ECM before being fully degraded by the extracellular nucleases [21]. The ECM consists of a structural collagen network embedded in a gel of glycosaminoglycans (GAGs) and proteoglycans. It is thought that treatment with agents that degrade the ECM components, hyaluronidase for example [20, 37], have the potential to increase the drugs penetration through the tissue and ultimately into cells [73]. They are therefore used in medicine to improve drugs dispersion and delivery [12].

DNA vaccination. There are several physical approaches to perform nonviral gene therapy. The simplest is the injection of naked DNA in the skeletal or cardiac muscle which leads to some expression of the injected genes [74]. However, this expression is very low and very variable from sample to sample. The main physical barrier encountered by DNA plasmids, the cell membrane, can be overcome using DNA electrotransfer [5]. But in the case of skeletal muscle, there is another limitation which is the access of the plasmid DNA to the muscle fiber surface. Controlled and partial degradation of ECM with matrix degrading enzymes is used to increase the diffusion and distribution of plasmid DNA into the muscle fiber. It has been shown that a pretreatment of skeletal muscle with hyaluronidase followed by DNA electrotransfer improves gene expression [63, 1, 61].

Chemotherapy. Delivery of drugs to tumor cells occurs by two independent mechanisms: diffusion and convection. However, the composition and structure of tumor-derived ECM can slow down the movement of therapeutic molecules within the tumor [33, 24, 49]. In addition, the disorganized vascular network and the absence of functional lymphatics cause increased interstitial fluid pressure (IFP), which is a major obstacle to transcapillary transport [7]. As far as diffusion is concerned, it was proven that an intratumoral injection of matrix degrading enzymes removes diffusive hindrance to the penetration of therapeutic molecules in tumor models [30, 36]. As far as convection is concerned, IFP may be temporarily reduced by degrading the tumor ECM. It has been shown that collagenase and hyaluronidase reduce IFP, thereby improving the uptake and distribution of molecules within solid tumors [28, 29, 19].

1.2 Main results

Need of numerical models. From the biological point of view, the effects of matrix degrading enzymes on drug transport is well known. However, the litterature suffers from a lack of models describing the active transport of those enzymes in the extracellular medium and the resulting changes on the ECM. The aim of this paper is to provide a mathematical model that addresses this phenomenon in order to offer a better understanding of the physical involved phenomena. The model consists of a non-linear system of partial differential equation (PDEs). It is derived directly from physical conservation laws. Constitutive relations are added to close the system. The derivation's steps are presented in Figure 2. We adopt a poroelastic approach to model the mechanics of a biological tissue. This choice is made to take into account the swelling of the tissue when fluid is added by injection. It is also in accordance with the studies stating that biological tissue deformations are not negligible in numerical models describing drug delivery [68]. This choice implies to first derive equations with Eulerian formalism and then reduce them to a fixed reference domain via a suitable change of variables in order to make the numerical processing possible. In addition, equations on the volume fractions of each component of the tissue are included to take into account the structural changes. In the end, the main variables of interest of the model are the three different volume fractions, the interstial pressure, the displacement and the concentrations of enzyme and therapeutic agent respectively. The final formulation of the model, system (55), is displayed in Section 3. To our knowledge, this is the first model describing the alteration of a poroelastic medium produced by chemical species injected directly in the medium. Alteration of a porous media is taken into account in [2, 58] but within a rigid structure. Many mathematical models of passive transport into a poroelastic medium do not take into account exchanges between phases [10, 68]. In [35, 46, 45], models including exchanges between phases are presented on closed poroelastic mixtures (no external sources or sinks). However, the changes are not mediated by external species. In [65, 66], magma is modeled as a poroelastic medium with varying porosity due to temperature changes. However, those changes are assumed to be infinitesimal. In [22, 6], poroelastic models taking into account ECM degradation by matrix degrading enzymes produced by tumor cells are presented within the particular framework of tumor growth. Nevertheless, these models have a very different focus, namely showing the formation of fibrosis. They also make slightly different assumptions: the ECM is rigid, the matrix degrading enzymes are produced by tumor cells and the cells' movement is the one of an elastic fluid. The goal of the paper is to derive a model that combines the effect of an injection of ECM degradation enzyme with a poroelastic macroscopic model of biological tissue (skeletal muscle or tumor tissue), and to provide a numerical method that allows to simulate the complete model in 1D-, 2D-, and axisymmetric configurations in order to compare the results with the qualitative data available in the litterature. Let us note that the long-term goal of the project is to provide a first step towards the numerical optimization of drug

delivery with enzyme pretreatment.

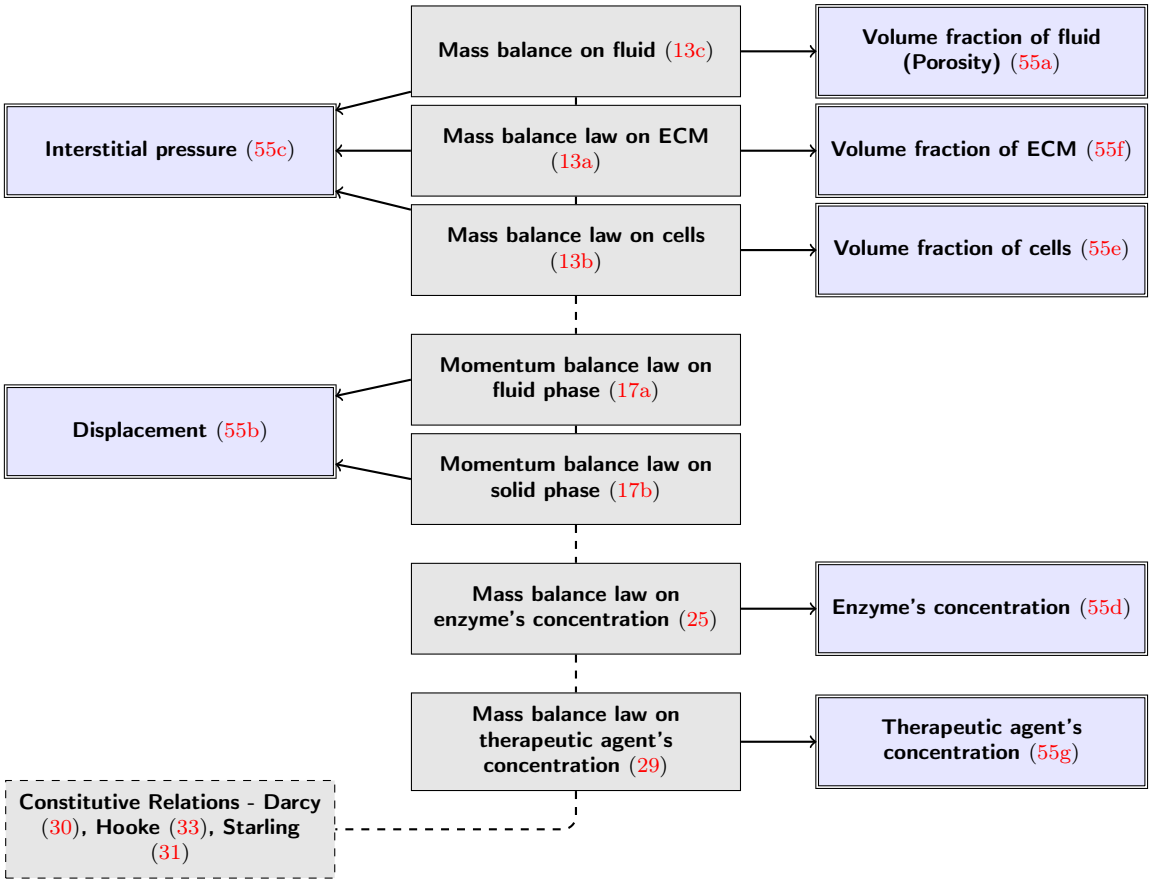

Figure 2: Schematic description of the derivation's method of the model. The first set of boxes contain the set of conservation laws and constitutive relations considered while the other boxes contain the final equations on the variables of interest derived from the physical laws. The numbering refers to the corresponding equations in their final form stated further in the article.

Numerical simulations illustrating biological phenomena. After testing the model with a set of numerical simulations to investigate the effect of the new parameters added (Figures 12 and 14), we use the model to describe two situations: the incubation of a spheroid into an ECM degradation enzyme and the intratumoral injection of enzyme in vivo. We observe that, in the first test case, given the dependency of the diffusion tensor on the porosity variable [48], a pretreatment with ECM degradation enzyme affects the distribution of therapeutic agents, thereby improving the diffusion process. Where without pretreatment, the macromolecules stay mainly at the periphery of the spheroid, a pretreatment with hyaluronidase permit to obtain a wider distribution (Figure 3).

In the second case, given the dependency of the pressure on the porosity variable, an intratumoral injection of enzyme results in a reduction of the IFP. This reduction depends on the enzyme's

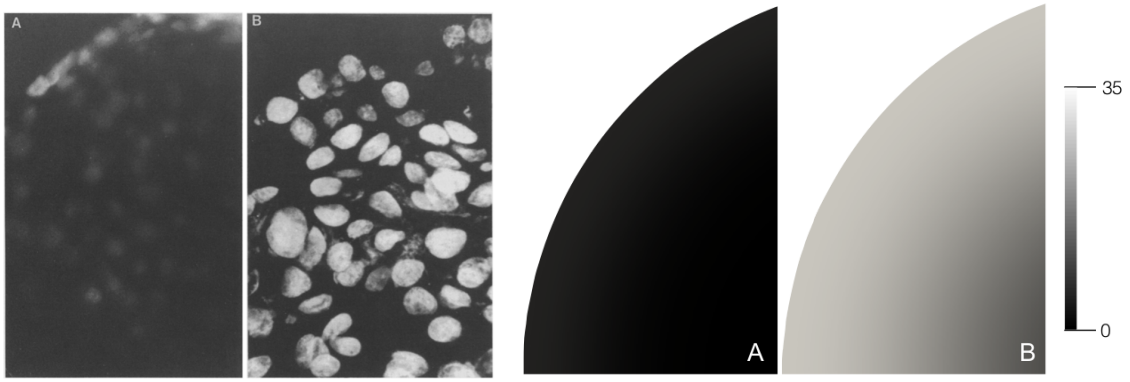

Figure 3: Comparison between experimental doxuribicin fluorescence (left, data from [43]) and numerically simulated (see Figure 18 in Section 5) concentration of anticancer agent in a spheroid previously incubated with hyaluronidase (B) or not (A).

concentration and reaches a maximum value, a further increase of the dose resulting in a smaller reduction, which is in accordance with the experiments (Figure 4).

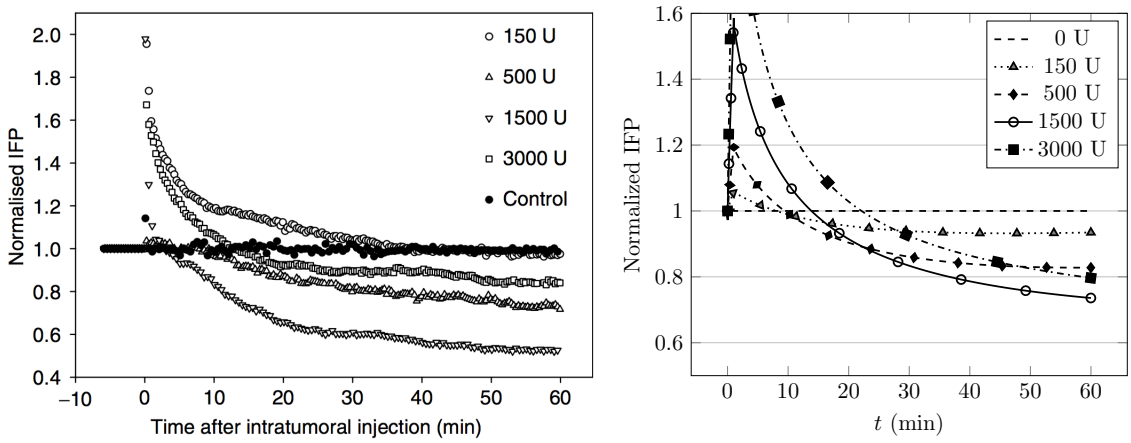

Figure 4: Comparison between experimental IFP (left, data from [29]) and numerically simulated IFP (see 5.3.4). Normalized interstitial fluid pressure is represented in both cases as a function of time after intratumoral injection of 150 U, 500 U, 1500 U and 3000 U hyaluronidase in tumors compared to no pretreatment (intratumoral injection of saline solution).

It also appears that a pretreatment with ECM degradation enzyme affects the distribution of therapeutic agents, thereby increasing its area of action by improving both the diffusion and the convection processes. This is once more in accordance with the experiments (data from [29]). Indeed, without pretreatment, the macromolecules stay only at the periphery of the tumor, the transcapillary transport being greatly reduced by the high IFP inside the tumor. A pretreatment with hyaluronidase permit to obtain a wider distribution. The molecules are thus distributed all over the tumor (Figure 5).

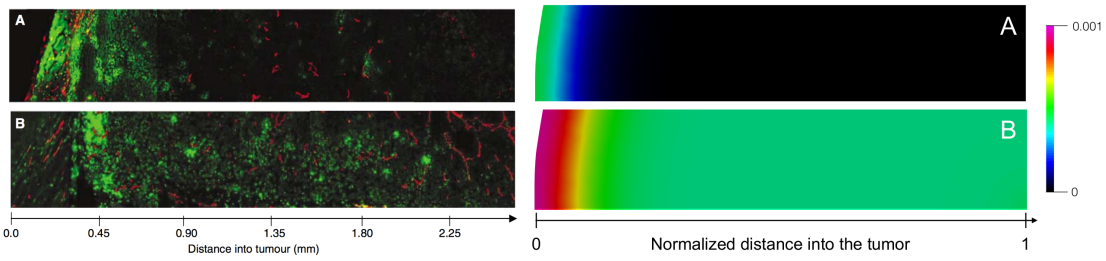

Figure 5: Comparison between experimental distribution of anticancer fluorescent agent (left, data from [29]) and numerically simulated concentration of agent. In case A, no pretreatment was previously performed on the tissue whereas in case B, the tissue was pretreated with 1500 U hyaluronidase.

1.3 Outline

In this paper, we construct a non-linear spatio-temporal model for the active transport of ECM degradation enzyme into a poroelastic biological tissue coupled with the passive transport of therapeutic agents. Section 2 is devoted to a precise description of our model following the scheme presented in Figure 2. It is divided in two parts: in the first part, we derive some equations from physical conservation laws, while in the second part, we conclude the formulation of our model stating some constitutive relations. Section 3 is devoted to the simplification of the model. We formulate the equations of the model in a fixed reference domain and assume a small displacement hypothesis that simplify the numerical processing. Section 4 contains the numerical scheme used to solve our PDE simplified model. The main features of the numerical model are then investigated in 1D- and 2D-configurations. We conclude by numerical simulations that corroborate experimental results in the framework of solid tumors in Section 5. To the best of our knowledge, it is the first time that a PDE model describes the effect of an injection of ECM degradation enzyme respectively on porosity, interstitial pressure and drug delivery. Calibration of the model with experimental data are planned in forthcoming works.

2 Derivation of the model

2.1 Framework

Modeling the behavior of porous media in which different continua interact at the microscopic level is not an easy task. In the current literature the mechanics of a porous medium is typically described by two different approaches: the averaging approach and the macroscopic approach [62], also known as mixture theory. The basic premise of the mixture theory is that the space occupied by a mixture is occupied co-jointly by the various constituents of the mixture, each considered as a continuum of its own. Thus, at any point of the space occupied by the mixture, there will be a particle belonging to each constituent [35].
We let $\mathbf{x}$ and t denote the space and time variables, respectively. To simplify notations, we omit the dependence of all variables and model parameters on $\mathbf{x}$ and t, except otherwise stated.
We denote by $\Omega_0 = \Omega(0) \subset \mathbb{R}^d$ $(d = 1, 2, 3)$ the initial spatial configuration, by $\Omega_t = \Omega(t)$ the configuration at time t and by T the final time of the experiment.
The biological tissue is considered as a binary mixture of a solid and an interstitial fluid. The

solid phase consists of cells and extracellular matrix (ECM). In what follows, the index ζ refers to one of the three constituents of the tissue: the fluid (f), the ECM ($\mathcal{E}$) or the cells ($\mathscr{c}$). The index s stands for the solid phase (ECM + cells). The density of the ζ^{th} constituent is denoted by ρ_ζ. It represents the mass of the ζ^{th} constituent per unit volume of the mixture. The density for the ζ^{th} constituent in a homogeneous state is denoted by ρ_ζ^R. It represents the mass of the ζ^{th} constituent per unit volume of the ζ^{th} constituent. The quantity defined by

$$\varphi_\zeta(t,\mathbf{x}) = \frac{\rho_\zeta(t,\mathbf{x})}{\rho_\zeta^R(t,\mathbf{x})}, \tag{1}$$

is the volume fraction of the mixture occupied by the ζ^{th} constituent. This definition coincides with the classic definition given by [14]. The following standard assumptions on the mixture are considered.

Assumption 1. (**Saturation**) The mixture is fully saturated, i.e.

$$\varphi_\mathcal{E} + \varphi_\mathscr{c} + \varphi_f = 1 \qquad \forall \mathbf{x} \in \Omega, \;\; \forall t > 0 \tag{2}$$

This saturation condition excludes the possibility of the formation of voids or air bubbles inside the medium.

Assumption 2. (**Incompressibility**) The liquid is incompressible in its pure state i.e. the density of the liquid in a homogeneous state is assumed to be a constant, namely

$$\rho_f^R(t,x) = \rho_f^{R,0}(t,x) \qquad \forall \mathbf{x} \in \Omega, \;\; \forall t > 0. \tag{3}$$

Assumption 3. All the solid matrix constituents (cells and ECM) have the same density in a homogeneous state:

$$\rho_\mathcal{E}^R(t,\mathbf{x}) = \rho_\mathscr{c}^R(t,\mathbf{x}) = \rho_s^R(t,\mathbf{x}). \tag{4}$$

Assumption 4. (**Slight compressibility**) The solid phase (ECM + cells) is slightly compressible in its pure state i.e. the density of the solid constituents in a homogeneous state can be written as [23]:

$$\rho_s^R(t,\mathbf{x}) = \rho_s^{R,0}(t,\mathbf{x})(1 + s_0(p(t,\mathbf{x}) - p(0,\mathbf{x}))), \qquad \forall \mathbf{x} \in \Omega, \;\; \forall t > 0, \tag{5}$$

where

$$s_0(p(t,\mathbf{x}) - p(0,\mathbf{x})) \ll 1, \qquad \forall \mathbf{x} \in \Omega, \;\; \forall t > 0, \tag{6}$$

and where p is the interstitial fluid pressure and where $\rho_s^{R,0}$ is a constant. s_0 can be related to the specific storage coefficient that appears in Biot's constitutive theory of consolidation [15].

Assumption 5. (**Mass exchanges**) We assume that mass exchanges occur only among cells/ECM and fluid, meaning that degrading ECM is detoriated into extracellular fluid, and conversely that the latter is consumed whenever ECM is created.

Assumption 6. (**Fluid source term**) Fluid is exchanged between interstitial space and the blood or lymph vessels: the fluid source term is then assumed to be driven by the average transmural pressure. If fluid is directly injected in the tissue, another external source of fluid is added during the injection.

2.2 Balance laws

In this section we give the set of conservation laws that constitute our proposed mathematical picture of the mechanobiological properties of the tissue using the Eulerian formalism. All the solid matrix constituents (cells and ECM) are experiencing the same motion. Thus $\mathbf{v}_{\mathcal{E}}(t,\mathbf{x}) = \mathbf{v}_{\varepsilon}(t,\mathbf{x}) = \mathbf{v}_s(t,\mathbf{x})$. The motion function refers to the solid phase, so it is useful to use the Eulerian velocity of the fluid with respect to the solid phase defined by

$$\mathbf{w}(t,\mathbf{x}) = \mathbf{v}_f(t,\mathbf{x}) - \mathbf{v}_s(t,\mathbf{x}). \tag{7}$$

2.2.1 Mass balance for each component of the mixture

The mass of the ζ^{th} constituent can change due to

1. the flux caused by the motion at the velocity $\mathbf{v}_\zeta$ of the constituent,
2. the production that accounts for possible mass conversion between constituents at a certain rate Q_ζ [35],
3. the source term $\mathcal{S}_\zeta$.

One then has

$$\frac{\partial \rho_\zeta}{\partial t} + \nabla\cdot(\rho_\zeta \mathbf{v}_\zeta) - \rho_\zeta Q_\zeta - \mathcal{S}_\zeta = 0, \tag{8}$$

where the source term $\mathcal{S}_\zeta$ is given as

$$\mathcal{S}_\zeta = \rho_\zeta^R \Sigma_\zeta. \tag{9}$$

Using definition (1) we get

$$\frac{\partial(\rho_\zeta^R \varphi_\zeta)}{\partial t} + \nabla\cdot(\rho_\zeta^R \varphi_\zeta \mathbf{v}_\zeta) - \rho_\zeta^R \varphi_\zeta Q_\zeta - \mathcal{S}_\zeta = 0.$$

To translate Assumption 5, we assume the following constraint [35]

$$\rho_s^R \varphi_{\mathcal{E}} Q_{\mathcal{E}} + \rho_f^R \varphi_f Q_f = 0. \tag{10}$$

The production terms Q_f and $Q_{\mathcal{E}}$ introduced here describe the mechanisms of addition and/or removal of mass for each species constituting an isolated tissue. We assume that the ECM is degraded proportionally to the enzyme's concentration [3], becoming fluid, and that the tissue recovers towards its initial state.
It is then relevant to choose the production term $Q_{\mathcal{E}}$ as

$$Q_{\mathcal{E}} = -K\varphi_f c_{\text{enz}} + a_r\left(\varphi_f - \varphi_f(0,\mathbf{x})\right). \tag{11}$$

where K is the rate of deterioration of the solid phase when in contact with the enzyme, represented by its concentration in the fluid phase $\varphi_f c_{\text{enz}}$. As the ECM is recovered a certain time after the injection of the enzyme [41, 38], the second term in the expression of $Q_{\mathcal{E}}$ represents this reconstitution of the tissue towards its initial state, at a certain rate of natural reconstruction a_r.
To translate Assumption 6, we choose the fluid source term as

$$\Sigma_f = Q_{\text{inj}}^{\text{tot}} + Q_{\text{vas}} - Q_{\text{lym}} \quad \text{where} \quad Q_{\text{inj}}^{\text{tot}} = Q_{\text{inj}}^{\text{enz}} + Q_{\text{inj}}^{\text{drug}}, \tag{12}$$

where $Q_{\text{inj}}^{\text{enz}}$ represents the injection term of enzyme, $Q_{\text{inj}}^{\text{drug}}$ represents the injection term of therapeutic agent, Q_{vas} is the transcapillary flow and Q_{lym} is the lymphatic drainage.

The mass balance equations for the tissue's constituents are then expressed by the following coupled system of PDEs in $\Omega_t \times (0,T)$:

$$\begin{cases} \dfrac{\partial}{\partial t}(\rho_s^R \varphi_{\mathcal{E}}) + \nabla \cdot (\rho_s^R \varphi_{\mathcal{E}} \mathbf{v}_s) = \rho_s^R \varphi_{\mathcal{E}} (-K \varphi_f c_{\text{enz}} + a_r (\varphi_f - \varphi_f(0,\mathbf{x}))), & \text{(13a)} \\ \dfrac{\partial}{\partial t}(\rho_s^R \varphi_{\mathcal{C}}) + \nabla \cdot (\rho_s^R \varphi_{\mathcal{C}} \mathbf{v}_s) = 0, & \text{(13b)} \\ \dfrac{\partial}{\partial t}(\rho_f^R \varphi_f) + \nabla \cdot (\rho_f^R \varphi_f \mathbf{v}_f) = \rho_s^R \varphi_{\mathcal{E}} (K \varphi_f c_{\text{enz}} - a_r (\varphi_f - \varphi_f(0,\mathbf{x}))) \\ \qquad\qquad + \rho_f^R (Q_{\text{inj}}^{\text{tot}} + Q_{\text{vas}} - Q_{\text{lym}}). & \text{(13c)} \end{cases}$$

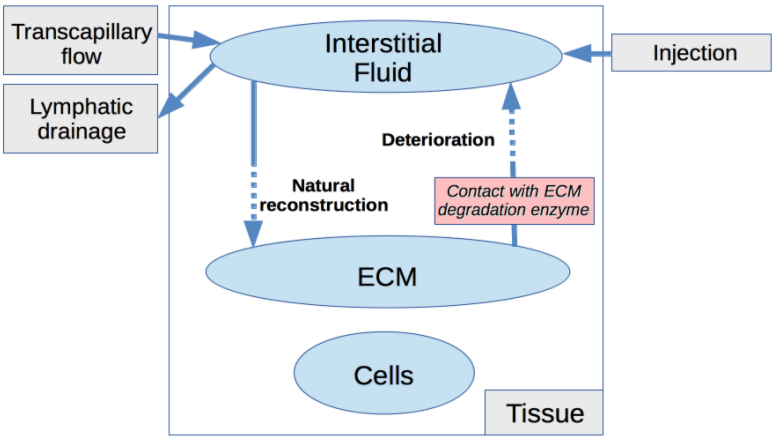

Figure 6: Schematic description of exchange pathways and production terms of the different phases.

2.2.2 Total mass balance for the mixture

Summing equations $(1/\rho_s^{R,0})\times$ (13a), $(1/\rho_s^{R,0})\times$ (13b) and $(1/\rho_f^R)\times$ (13c), using Assumptions 1 and 3, and conditions (6)-(10) we get

$$\begin{aligned} \varphi_s s_0 \left(\frac{\partial p}{\partial t} + \nabla p \cdot \mathbf{v}_s \right) + \nabla \cdot (\varphi_s \mathbf{v}_s + \varphi_f \mathbf{v}_f) &= Q_{\text{inj}}^{\text{tot}} + Q_{\text{vas}} - Q_{\text{lym}} \\ + \left(1 - \frac{\rho_s^{R,0}}{\rho_f^R} \right) \varphi_{\mathcal{E}} (-K \varphi_f c_{\text{enz}} + a_r (\varphi_f - \varphi_f(0,\mathbf{x}))). & \end{aligned} \tag{14}$$

This equation expresses the conservation of the total mass of the tissue. A simple manipulation allows us to write (14) as

$$\begin{aligned} \varphi_s s_0 \left(\frac{\partial p}{\partial t} + \nabla p \cdot \mathbf{v}_s \right) + \nabla \cdot (\mathbf{v}_s + \varphi_f \mathbf{w}) &= Q_{\text{inj}}^{\text{tot}} + Q_{\text{vas}} - Q_{\text{lym}} \\ + \left(1 - \frac{\rho_s^{R,0}}{\rho_f^R} \right) \varphi_{\mathcal{E}} (-K \varphi_f c_{\text{enz}} + a_r (\varphi_f - \varphi_f(0,\mathbf{x}))). & \end{aligned} \tag{15}$$

Remark 1. The term $\varphi_s s_0 \left(\frac{\partial p}{\partial t} + \nabla p \cdot \mathbf{v}_s\right)$ in Equation (15) comes from Assumptions 5 and 6. If the density in an homogeneous state of the solid phase were assumed to be a constant, this term would vanish.

2.2.3 Momentum balance for each component of the mixture

The momentum of the ζ^{th} constituent can change due to

1. the momentum flux caused by the motion at the velocity $\mathbf{v}_\zeta$ of the constituent,
2. contact forces within the constituent acting through the boundary,
3. contact forces due to the interaction with the other constituents within the domain through the interface separating the constituents,
4. momentum supply related to phase changes,
5. momentum supply related to external sources or sinks of mass,
6. body forces.

One can then write the following local form of the momentum balance in conservative form

$$\frac{\partial}{\partial t}(\rho_\zeta \mathbf{v}_\zeta) + \boldsymbol{\nabla} \cdot (\rho_\zeta \mathbf{v}_\zeta \otimes \mathbf{v}_\zeta) = \boldsymbol{\nabla} \cdot \boldsymbol{\sigma}_\zeta + \rho_\zeta \mathbf{b} + \boldsymbol{\pi}_\zeta + \rho_\zeta Q_\zeta \mathbf{v}_\zeta + \mathcal{S}_\zeta \mathbf{v}_\zeta,$$

where

- $\boldsymbol{\sigma}_\zeta$ is called the partial stress,
- $\boldsymbol{\pi}_\zeta$ is called the interaction force,
- $\mathbf{b}$ is an external force applied to the system e.g., extra pressure due to the injection.

Actually using the mass balance equation (8), this equation can be simplified as

$$\rho_\zeta \left(\frac{\partial}{\partial t}\mathbf{v}_\zeta + \mathbf{v}_\zeta \cdot \boldsymbol{\nabla}\mathbf{v}_\zeta\right) = \boldsymbol{\nabla} \cdot \boldsymbol{\sigma}_\zeta + \rho_\zeta \mathbf{b} + \boldsymbol{\pi}_\zeta, \tag{16}$$

where the inertial term on the left-hand side can usually be neglected when describing biological tissues [8, 9]. Let's recall that all the solid matrix constituents (cells and ECM) experience the same overall motion, so we can simplify the momentum balance equations for the tissue's constituents into the a coupled system of PDEs to be solved in $\Omega_t \times (0, T)$:

$$\begin{cases} \boldsymbol{\nabla} \cdot \boldsymbol{\sigma}_f + \rho_f^R \varphi_f \mathbf{b} + \boldsymbol{\pi}_f = 0, & \text{(17a)} \\ \boldsymbol{\nabla} \cdot \boldsymbol{\sigma}_s + \rho_s^R \varphi_s \mathbf{b} + \boldsymbol{\pi}_s = 0, & \text{(17b)} \end{cases}$$

where (17b) is the equation resulting from the sum of (16) for $\zeta = \mathcal{E}, \mathcal{c}$, and expresses the total momentum of the solid phase as a whole. In the case of a saturated mixture, it can be proved that [18]

$$\begin{cases} \boldsymbol{\sigma}_s = -\varphi_s p \mathbf{I} + \varphi_s \boldsymbol{\sigma}_s^E & \text{(18a)} \\ \boldsymbol{\sigma}_f = -\varphi_f p \mathbf{I} & \text{(18b)} \end{cases}$$

where $\boldsymbol{\sigma}_s^E$ is the effective stress tensor of the solid phase of the tissue, whose form will be discussed in Section 2.3, and where $p = p(t, \mathbf{x})$ is the pressure exerted by the fluid phase and $\mathbf{I}$ is

the identity tensor. The isotropic stress $-p\mathbf{I}$ accounts for the coupling, typical of poroelasticity, between the low of the fluid and the deformation of the solid matrix, and in particular describes the contribution to the stress due to the fluid pressure within the structure.
The quantities $\boldsymbol{\sigma}_\zeta$, $\zeta = s, f$, are the total stress tensors of the solid and fluid phases. As usual, we neglect the effective stress tensor of the fluid, meaning that we assume that the internal fluid viscosity is negligible compared with the friction between the fluid and the solid matrix [9].
We observe that, for all $t \in (0, T)$ and at all $\mathbf{x} \in \Omega$, it holds [57]

$$\boldsymbol{\pi}_s(t, \mathbf{x}) + \boldsymbol{\pi}_f(t, \mathbf{x}) = 0. \tag{19}$$

2.2.4 Total momentum balance for the mixture

Summing equations (16) for $\zeta = s, f$ and using (18), we get

$$\boldsymbol{\nabla} \cdot (\varphi_s \boldsymbol{\sigma}_s^E) + (\rho_f + \rho_s)\mathbf{b} = \nabla p. \tag{20}$$

This equation expresses the conservation of total momentum of the tissue. In what follows, we will assume the external body forces to be zero, such that equation (20) becomes

$$\boldsymbol{\nabla} \cdot (\varphi_s \boldsymbol{\sigma}_s^E) = \nabla p. \tag{21}$$

2.2.5 Mass balance for ECM degradation enzyme's concentration

Another fundamental quantity of interest from the modeling point of view is the concentration in ECM degradation enzyme, such as hyaluronidase or collagenase, per unit volume within the fluid phase of the tissue, $c_{\text{enz}} = c_{\text{enz}}(t, \mathbf{x})$. However, the concentration c_{enz} has to be related to the volume ratio occupied by the interstitial fluid. Finally the relevant entity for an overall balance over the whole tissue is the *reduced (or weighted) concentration*, e.g. $C_{\text{enz}} = \varphi_f c_{\text{enz}}$.
The mass balance system (13) for the solid and fluid phases of the tissue is thus accompanied by a corresponding continuity equation for the hyaluronidase concentration that is transported throughout the tissue by the interstitial fluid. We consider that the reduced concentration can change due to

1. the motion of the fluid at the velocity $\mathbf{v}_f$,
2. the diffusive flux,
3. natural degradation and/or the intake due to the source.

Therefore, the following reaction-convection-diffusion equation reads

$$\frac{\partial}{\partial t}(\varphi_f c_{\text{enz}}) + \nabla \cdot (\varphi_f c_{\text{enz}} \mathbf{v}_f) = -\nabla \cdot (\varphi_f \mathbf{j}_{\text{enz}}^f) - k_{\text{enz}}^{d,\text{eff}} \varphi_f c_{\text{enz}} + \mathcal{S}_{\text{enz}}, \tag{22}$$

where

- $\mathbf{j}_{\text{enz}}^f$ is diffusive flux inside the liquid phase,
- $k_{\text{enz}}^{d,\text{eff}}$ is the net natural degradation effective rate of the enzyme in the interstitial fluid,
- $\mathcal{S}_{\text{enz}}$ is the contribution consecutive to the injection (directly into the tissue or intravenously) of enzyme.

Fick's law states that the diffusive flux can be assumed to be proportional to the concentration gradient in the liquid, that is

$$\mathbf{j}^f_{\text{enz}} = -\mathbf{D}^f_{\text{enz}} \nabla c_{\text{enz}}, \tag{23}$$

where $\mathbf{D}^f_{\text{enz}}$ is the effective diffusion tensor in the liquid, that we choose to be a tensor linearly dependent on the porosity [48]

$$\mathbf{D}^f_{\text{enz}} = \varphi_f \mathbf{D}^0_{\text{enz}}. \tag{24}$$

Hence, equation (22) in terms of $C_{\text{enz}} = \varphi_f c_{\text{enz}}$ becomes

$$\frac{\partial C_{\text{enz}}}{\partial t} + \nabla \cdot (C_{\text{enz}} \mathbf{v}_f) = \nabla \cdot \left(\varphi_f^2 \mathbf{D}^0_{\text{enz}} \nabla \left(\frac{C_{\text{enz}}}{\varphi_f} \right) \right) - k^{d,\text{eff}}_{\text{enz}} C_{\text{enz}} + \mathcal{S}_{\text{enz}}. \tag{25}$$

2.2.6 Mass balance for drug concentration

The main quantity of interest from the modeling point of view is the concentration in therapeutic agent per unit volume within the fluid phase of the tissue, $c_{\text{drug}} = c_{\text{drug}}(t, \mathbf{x})$. As previously, the concentration c_{drug} has to be related to the volume ratio the interstitial fluid. The relevant entity for an overall balance over the whole tissue is the *reduced (or weighted) concentration*, e.g. $C_{\text{drug}} = \varphi_f c_{\text{drug}}$. The continuity equation for the therapeutic agent's concentration that is transported throughout the tissue by the interstitial fluid can be deduced considering that the reduced concentration can change due to

1. the motion of the fluid
2. the diffusive flux
3. natural degradation and/or the intake due to the source.

Therefore, the following reaction-convection-diffusion equation can be deduced

$$\frac{\partial}{\partial t}(\varphi_f c_{\text{drug}}) + \nabla \cdot (\varphi_f c_{\text{drug}} \mathbf{v}_f) = -\nabla \cdot (\varphi_f \mathbf{j}^f_{\text{drug}}) - k^{d,\text{eff}}_{\text{drug}} \varphi_f c_{\text{drug}} + \mathcal{S}_{\text{drug}}, \tag{26}$$

where

- $\mathbf{j}^f_{\text{drug}}$ is diffusive flux inside the liquid phase,
- $k^{d,\text{eff}}_{\text{drug}}$ is the net natural degradation effective rate of the drug in the interstitial fluid,
- $\mathcal{S}_{\text{drug}}$ is the contribution consecutive to the injection (directly into the tissue or intravenously) of drug.

As before, Fick's law states that the diffusive flux can be assumed to be proportionnal to the concentration gradient in the liquid, that is

$$\mathbf{j}^f_{\text{drug}} = -\mathbf{D}^f_{\text{drug}} \nabla c_{\text{drug}}, \tag{27}$$

where $\mathbf{D}^f_{\text{drug}}$ is the effective diffusion coefficient in the liquid, that we choose to be linearly dependent on the porosity [48]

$$\mathbf{D}^f_{\text{drug}} = \varphi_f \mathbf{D}^0_{\text{drug}}. \tag{28}$$

Hence, using (13c), equation (22) simplifies to

$$\frac{\partial C_{\text{drug}}}{\partial t} + \nabla \cdot (C_{\text{drug}} \mathbf{v}_f) = \nabla \cdot \left(\varphi_f^2 \mathbf{D}^0_{\text{drug}} \nabla \left(\frac{C_{\text{drug}}}{\varphi_f} \right) \right) - k^{d,\text{eff}}_{\text{drug}} C_{\text{drug}} + \mathcal{S}_{\text{drug}}. \tag{29}$$

2.3 Constitutive equations regarding the mechanical and fluid subsystems

2.3.1 Darcy's law

We assume the relative velocity to be expressed by Darcy's law [4, 10, 6, 9]

$$\varphi_f \mathbf{w} = \varphi(\mathbf{v}_f - \mathbf{v}_s) = -\boldsymbol{\kappa}\nabla p \tag{30}$$

where $\boldsymbol{\kappa}$ is the permeability tensor.

2.3.2 Starling's law

The transcapillary flow and the lymphatic drainage are taken into account in (12). Both rates Q_{vas} and Q_{lym} can be evaluated throught Starling's law. A complete description of the formulation of this law can be found in [64]. The final result is

$$Q_{\text{vas}} - Q_{\text{lym}} = \frac{L_p S + L_{PL} S_L}{V}(p_v - p), \tag{31}$$

where L_p and L_{PL} are the hydraulic conductivities of the microvascular wall and of the lymphatic wall respectively; S/V and S_L/V are the surface area per unit volume of the vasculature and of the lymphatics respectively; and where p_v is the driving pressure. Equation (31) will be written as

$$Q_{\text{vas}} - Q_{\text{lym}} = \gamma(p_v - p), \tag{32}$$

where $\gamma = (L_p S + L_{PL} S_L)/V$ will be assumed to be a constant.

2.3.3 The linear elasticity framework

To complete our derivations of the equations of motion, we must know (or assume) the relationships (constitutive laws) between effective stress and strain. The classical theory of elasticity deals with the mechanical properties of elastic solids for which the stress is directly proportional to the stress in small deformations. Linear elastic theory can be satisfactorily applied for modeling the mechanical properties of biological media [34, 50, 10, 16]: namely, we assume that biological tissues are nearly linear elastic under small strain and follow a constitutive law based on Hooke's law. Specifically, a Hookean elastic solid is a solid that obeys Hooke's Law, that states that the first Piola-Kirchhoff stress tensor $\mathbf{S}_s^E$ is such that

$$\mathbf{S}_{s;ij}^E = C_{ijkl}\boldsymbol{\varepsilon}_{kl} \tag{33}$$

where C_{ijkl} is the stiffness tensor and where $\boldsymbol{\varepsilon}$ is the infinitesimal strain (48) defined later in Section 3.

Remark 2. For most materials, the linear elasticity framework is only valid for small displacements [59].

Remark 3. In biomechanics, biological tissues are thought to be better described as viscoelastic solids [34, 27]. However, for the sake of simplicity, we choose here to stay within the framework of the linear elasticity theory.

The first Piola-Kirchhoff stress tensor is then related to the Cauchy stress tensor [11] via the deformation gradient A (47) defined in Section 3

$$\boldsymbol{\sigma}_s^E = \frac{1}{J} A \mathbf{S}_s^E A^T. \tag{34}$$

Isotropic media. In the most simple symmetry case of an isotropic elastic solid, the material has only two independent elastic moduli, called the Lamé constants, λ and μ . In such a medium the elastic properties at any point are independent from direction. The Lamé constants are related to the stiffness tensor C_{ijkl} by

$$C_{ijkl} = \lambda\delta_{ij}\delta_{kl} + \mu\left(\delta_{ik}\delta_{jl} + \delta_{il}\delta_{jk}\right),$$

which gives us the following form for the effective stress $\mathbf{S}_s^E$

$$\mathbf{S}_s^E = 2\mu\boldsymbol{\varepsilon} + \lambda Tr(\boldsymbol{\varepsilon})I_d. \tag{35}$$

As far as the diffusion tensors and the permeability tensor are concerned, in the isotropic case, we take

$$\mathbf{D}^0_{\text{enz}} = D^0_{\text{enz}} I_d, \qquad \mathbf{D}^0_{\text{drug}} = D^0_{\text{drug}} I_d, \qquad \boldsymbol{\kappa} = \kappa I_d. \tag{36}$$

Transverse isotropic media. It is now well established that anisotropy plays a major role in the mechanical properties of biological media such as muscles, tendons or bones [60]. The most simple anisotropic model is the transverse isotropy. A transversely isotropic tissue is characterized by the existence of a single plane of isotropy and one single axis of rotational symmetry, the normal to the isotropy plane. Skeletal muscle, for instance, consists of hundreds to thousands, sometimes millions, of long, multinucleated fibers organized and held together by an ECM thus it is relevant to model it as a transverse isotropic media.
In the case of a transverse isotropic medium in 2D, relation (33) reduces to (35) in the plane of isotropy (xy). If we consider the plane (xz), (33) can be written in the following fashion

$$\begin{pmatrix} \mathbf{S}^E_{s;11} \\ \mathbf{S}^E_{s;33} \\ \mathbf{S}^E_{s;13} \end{pmatrix} = \begin{pmatrix} C_{1111} & C_{1133} & 0 \\ C_{1133} & C_{3333} & 0 \\ 0 & 0 & C_{1313} \end{pmatrix} \begin{pmatrix} \varepsilon_{11} \\ \varepsilon_{33} \\ 2\varepsilon_{13} \end{pmatrix}. \tag{37}$$

It has been reported [70] that the permeability $\boldsymbol{\kappa}$ depends on many factors including the geometry. Orientation can affect $\boldsymbol{\kappa}$, with perpendicular fibers providing a larger resistance to flow $\kappa_\perp$ than parallel fibers $\kappa_{/\!/}$. Consequently, in a rightful vector basis, we take $\boldsymbol{\kappa}$ as

$$\boldsymbol{\kappa} = \begin{pmatrix} \kappa_{/\!/} & 0 \\ 0 & \kappa_\perp \end{pmatrix}. \tag{38}$$

As far as the diffusion tensors are concerned, it was also reported [25, 26] that the diffusion coefficient parallel to a skeletal muscle fiber's long axis $D^0_{\text{enz},/\!/}$ (resp. $D^0_{\text{drug},/\!/}$) is greater than the diffusion coefficient perpendicular to the fiber's long axis $D^0_{\text{enz},\perp}$ (resp. $D^0_{\text{drug},\perp}$). Consequently, in a rightful vector basis,

$$\mathbf{D}^0_{\text{enz}} = \begin{pmatrix} D^0_{\text{enz},/\!/} & 0 \\ 0 & D^0_{\text{enz},\perp} \end{pmatrix}, \quad \text{resp. } \mathbf{D}^0_{\text{drug}} = \begin{pmatrix} D^0_{\text{drug},/\!/} & 0 \\ 0 & D^0_{\text{drug},\perp} \end{pmatrix}. \tag{39}$$

2.3.4 Degradation rates

The degree of porosity has a significant impact on the net natural degradation effective rate of the enzyme or the drug in the interstitial fluid $k^{d,\text{eff}}_{\text{enz}}, k^{d,\text{eff}}_{\text{drug}}$. The effects are both attributed to a wall effect and a surface area effect because the media with lower porosities or larger pores

possess thicker pore walls and smaller surface area, which depress the diffusion of degradation products [75]. Consequently, we choose

$$k_{\text{enz}}^{d,\text{eff}} = \frac{k_{\text{enz}}^{d}}{\varphi_f} \text{ and } k_{\text{drug}}^{d,\text{eff}} = \frac{k_{\text{drug}}^{d}}{\varphi_f}, \tag{40}$$

where k_{enz}^{d} and k_{drug}^{d} are positive constants.

2.3.5 Source terms.

Let the index ω denote either of the chemical species of interest (enzyme and/or drug).

Injection. If the chemical specie is directly injected in the tissue, we can choose to take the source term as

$$\mathcal{S}_\omega = c_{\text{inj}}^{\omega} Q_{\text{inj}}^{\omega}, \tag{41}$$

where c_{inj}^{ω} is the value of the specie concentration injected, which is assumed to be a constant. In the numerical simulations of sections 4 and 5, Q_{inj}^{ω} is a Gaussian function with a very small spread

$$Q_{\text{inj}}^{\omega} = q_{\text{inj}}^{\omega} \exp\left(-\sum_{i=1}^{d} \frac{(x_i - x_i^0)^2}{2\sigma_{x_i}^2} \right), \tag{42}$$

where $q_{\text{inj}}^{\omega}, \sigma_{x_i}$ are positive constants and where $(x_1^0, \ldots, x_d^0)$ indicate the coordinates of the injection point.

Incubation. If the tissue is incubated in the chemical specie, the source term $\mathcal{S}_\omega$ is taken as zero and and we choose instead to apply a non homogeneous Dirichlet boundary condition on C_ω (cf section 5).

Transcapillary transport. If the chemical specie is injected intravenously, we choose to take the source term accordingly with the pore model for transcapillary exchange via convection stated in [13]

$$\mathcal{S}_\omega = (1 - \gamma_c)(Q_{\text{vas}} - Q_{\text{lym}}) c_v^{\omega}, \tag{43}$$

where γ_c represents the coupling between fluid and solute and c_v^{ω} is the plasma concentration of the chemical specie. In the numerical simulations of section 5, for the sake of simplicity,

$$c_v^{\omega} = c_{v,0}^{\omega} \, \chi_{|t_1 \le t \le t_2}, \tag{44}$$

where $c_{v,0}^{\omega}$ is a constant, and $[t_1, t_2]$ is the time interval of presence in the capillary network. c_v^{ω} can be chosen to follow any pharmacokinetic model of interest.

3 Formulation of the poroelastic model in a fixed domain

3.1 Kinematics of the mixture

The motion of the constituents is described by the position occupied at time t by the particle labelled $\mathbf{X}$

$$\mathbf{x} = \Phi(t, \mathbf{X}), \tag{45}$$

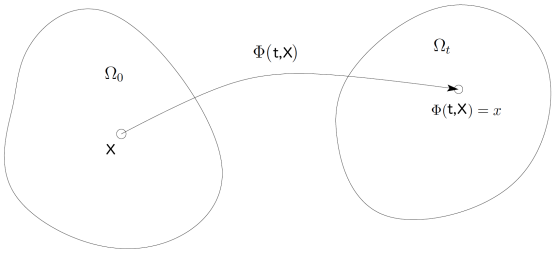

Figure 7: Deformation from the fixed domain Ω_0 via the application Φ

$\mathbf{X}$ being the position of the particle in the reference configuration Ω_0. The function $\Phi(t,.)$ represents a mapping from initial (undeformed) configuration Ω_0 to the present (deformed) configuration Ω_t.
The velocity of a particle belonging to the ζ^{th} constituent, often termed the Lagrangian velocity, $\mathbf{V}_\zeta(t,\mathbf{X})$, is the time rate change of the particle position holding $\mathbf{X}$ fixed. As we will use the Eulerian formalism to state conservation equations, we recall that the Eulerian velocity at time t and position $\mathbf{x}$, $\mathbf{v}_\zeta(t,\mathbf{x})$, is given by

$$\mathbf{v}_\zeta(t,\mathbf{x}) = \mathbf{V}_\zeta(t,\mathbf{X}) \text{ when } \mathbf{x} = \Phi(t,\mathbf{X}). \tag{46}$$

The configuration gradient, or deformation gradient, is defined by

$$A := \frac{\partial \mathbf{x}}{\partial \mathbf{X}} = \left(\frac{\partial x_i}{\partial X_j}\right)_{i,j=1..d} \tag{47}$$

We also set $B := A^{-1}$ and $J := \det(A)$. We stated that all the solid matrix constituents (cells and ECM) experience the same overall motion [45]. The displacement vector of the solid phase will be denoted $\mathbf{u} = \mathbf{u}(t,\mathbf{X})$. Note that we then have

$$\mathbf{V}_s(t,\mathbf{X}) = \frac{\partial}{\partial t}\mathbf{u}(t,\mathbf{X}).$$

We also define the associated infinitesimal deformation of the volume surrounding the point $\mathbf{X}$ at time t as

$$\boldsymbol{\varepsilon}(t,\mathbf{X}) = \frac{1}{2}\left(\nabla\mathbf{u}(t,\mathbf{X}) + (\nabla\mathbf{u}(t,\mathbf{X})^T\right). \tag{48}$$

It is also useful to define the material time derivative following the solid matrix

$$\frac{D(.)}{Dt} = \frac{\partial(.)}{\partial t} + (\mathbf{v}_s.\nabla)(.). \tag{49}$$

3.2 Change of variables

From now on, the medium is assumed to be isotropic. The formulation in a transverse isotropic medium will be similar as only equation (55b) will change. To reduce the governing equations to the reference fixed domain Ω_0, we introduce a suitable change of variable, which is given by the motion function (45): $\mathbf{x} = \Phi(t,\mathbf{X})$.
If $\mathbf{u}(t,\mathbf{X}) = \mathbf{x} - \mathbf{X}$ is the displacement vector, Φ is given by

$$\Phi(t,\mathbf{X}) = \mathbf{X} + \mathbf{u}(t,\mathbf{X}). \tag{50}$$

Let us set

$$
\begin{aligned}
&f(t,\mathbf{X}) := \varphi_f(t,\Phi(t,\mathbf{X})),\ g_s(t,\mathbf{X}) := \varphi_s(t,\Phi(t,\mathbf{X})),\\
&g_{\mathcal{E}}(t,\mathbf{X}) := \varphi_{\mathcal{E}}(t,\Phi(t,\mathbf{X})),\ g_c(t,\mathbf{X}) := \varphi_c(t,\Phi(t,\mathbf{X})),\\
&P(t,\mathbf{X}) := p(t,\Phi(t,\mathbf{X})),\ P_v(t,\mathbf{X}) := p_v(t,\Phi(t,\mathbf{X})),\\
&h(t,\mathbf{X}) := C_{\text{enz}}(t,\Phi(t,\mathbf{X})),\ c(t,\mathbf{X}) := C_{\text{drug}}(t,\Phi(t,\mathbf{X})),
\end{aligned}
$$

Recall that we have already from Section 2.3

$$
\mathbf{v}_s(t,\mathbf{x}) = \mathbf{V}_s(t,\mathbf{X}) = \frac{\partial}{\partial t}\mathbf{u}(t,\mathbf{X}), \tag{51}
$$

and

$$
\boldsymbol{\sigma}_s^E = \frac{1}{J}B^{-1}\mathbf{S}_s^E B^{-T} \text{ with } \mathbf{S}_s^E = 2\mu\boldsymbol{\varepsilon} + \lambda Tr(\boldsymbol{\varepsilon})I_d, \tag{52}
$$

since we consider the isotropic case. Moreover, every time and space derivative are affected by the change of variables in the following fashion (example on $f = \varphi_f$):

$$
\frac{D\varphi_f}{Dt} = \frac{\partial f}{\partial t},\ \ \nabla_{\mathbf{x}}\varphi_f = B\,\nabla_{\mathbf{X}} f. \tag{53}
$$

3.3 Non-dimensionalization

We state that from now ∇ denotes the operator $\nabla_{\mathbf{X}} = (\partial_{X_1},\dots,\partial_{X_d})^T$. Denote by l_0 the typical length of the porous medium. We non-dimensionalize the governing equations by letting

$$
\begin{aligned}
&\mathbf{X} = l_0\overline{\mathbf{X}}, \qquad \mathbf{u} = l_0\overline{\mathbf{u}}, \quad t = \frac{l_0^2}{\kappa(\lambda+2\mu)}\bar{t}, \quad \mathbf{V}_s = \frac{\kappa(\lambda+2\mu)}{l_0}\overline{\mathbf{V}_s},\\
&P = (\lambda+2\mu)\overline{P}, \quad h = c_0\overline{h}, \quad c = c_0\overline{c},
\end{aligned}
$$

where we use bars to denote the dimensionless variables. The dimensionless Piola-Kirchhoff and Cauchy stress tensors are defined as $\overline{\mathbf{S}_s^E} = \mathbf{S}_s^E/(\lambda+2\mu)$ and $\overline{\boldsymbol{\sigma}_s^E} = \boldsymbol{\sigma}_s^E/(\lambda+2\mu)$, respectively, and we define the dimensionless parameters

$$
\begin{aligned}
&\overline{\mu} = \frac{\mu}{\lambda+2\mu}, && \overline{\lambda} = \frac{\lambda}{\lambda+2\mu}, && \overline{s_0} = s_0(\lambda+2\mu), && \overline{\boldsymbol{\kappa}} = \frac{1}{\kappa}\boldsymbol{\kappa},\\
&\alpha = \frac{l_0^2}{\kappa(\lambda+2\mu)}, && \overline{K} = \alpha c_0 K, && \overline{a_r} = \alpha a_r, && \overline{\gamma} = \frac{l_0^2}{\kappa}\gamma,\\
&\overline{\mathbf{D}^0_{\text{enz}}} = \frac{1}{\kappa(\lambda+2\mu)}\mathbf{D}^0_{\text{enz}}, && \overline{k^d_{\text{enz}}} = \alpha k^d_{\text{enz}}, && \overline{P_v} = \frac{P_v}{\lambda+2\mu},\\
&\overline{\mathbf{D}^0_{\text{drug}}} = \frac{1}{\kappa(\lambda+2\mu)}\mathbf{D}^0_{\text{drug}}, && \overline{k^d_{\text{drug}}} = \alpha k^d_{\text{drug}}.
\end{aligned}
$$

We choose the $(\lambda+2\mu)$ parameter as a natural pressure scale; by this choice the dimensionless elastic parameters $\overline{\lambda}, \overline{\mu}$ are of order 1 [44].

3.4 Simplification of the model

The governing equations in Ω_t can be reformulated on the fixed reference domain Ω_0 dimensionless. The first advantage of this process is to obtain a system of equations in a fixed reference domain in order to make the numerical processing possible. Second, the constitutive relation on the stress tensor $\mathbf{S}_s^E$ is given in the lagrangian coordinates $(t, \mathbf{X})$, so it is natural to work within this system of coordinates. The third benefit is to elude the transport equations of the three different volume fractions: in the fixed reference domain, those equations reduce to ordinary differential equations. In particular, we don't have to state boundary conditions on the porosity. The calculus in the general case can be found in Appendix A. For the sake of simplicity, we will assume that our system undergo very small perturbations (see Remark 2). One can see then that $B = I_d + \mathcal{M}(\nabla \mathbf{u})$, where in the case of very small deformations, the coefficients of matrix $\mathcal{M}(\nabla \mathbf{u})$ are negligible before 1. Thus we can write the system with $B = I_d$. Let us denote

$$J_{\text{enz}} = \frac{1}{f}\overline{\boldsymbol{\kappa}}\,\nabla P - \overline{\mathbf{D}^0_{\text{enz}}}\nabla f \qquad \text{and} \qquad J_{\text{drug}} = \frac{1}{f}\overline{\boldsymbol{\kappa}}\,\nabla P - \overline{\mathbf{D}^0_{\text{drug}}}\nabla f. \tag{54}$$

The equivalent system in Ω_0 in dimensionless form in this simplified case reads

$$\begin{cases}
g_{\mathcal{E}} + g_{\mathcal{C}} + f = 1, & \text{(55a)}\\
\boldsymbol{\nabla}\cdot\left((g_{\mathcal{E}} + g_{\mathcal{C}})\left(\overline{\lambda}(\nabla\cdot\mathbf{u})I + \overline{\mu}(\nabla\mathbf{u} + \nabla\mathbf{u}^T)\right)\right) = \nabla P, & \text{(55b)}\\
(g_{\mathcal{E}} + g_{\mathcal{C}})\overline{s_0}\dfrac{\partial P}{\partial t} - \nabla\cdot(\overline{\boldsymbol{\kappa}}\,\nabla P) = \alpha\, Q^{\text{tot}}_{\text{inj}} + \overline{\gamma}(\overline{P_v} - P) \\
\qquad + \left(\dfrac{\rho_s^{R,0}}{\rho_f^R} - 1\right) g_{\mathcal{E}}(\overline{K}h + \overline{a_r}(f(0,\mathbf{x}) - f)) - \nabla\cdot\left(\dfrac{\partial \mathbf{u}}{\partial t}\right), & \text{(55c)}\\
\dfrac{\partial h}{\partial t} = \nabla\cdot(f\overline{\mathbf{D}^0_{\text{enz}}}\nabla h + hJ_{\text{enz}}) + h\left(-\dfrac{\overline{k^d_{\text{enz}}}}{f} - \nabla\cdot\left(\dfrac{\partial \mathbf{u}}{\partial t}\right)\right) + \dfrac{\alpha\mathcal{S}_{\text{enz}}}{c_0}, & \text{(55d)}\\
\dfrac{\partial g_{\mathcal{C}}}{\partial t} + \left(\overline{s_0}\dfrac{\partial P}{\partial t} + \nabla\cdot\left(\dfrac{\partial \mathbf{u}}{\partial t}\right)\right) g_{\mathcal{C}} = 0, & \text{(55e)}\\
\dfrac{\partial g_{\mathcal{E}}}{\partial t} + \left(\overline{K}h + \overline{a_r}(f(0,\mathbf{x}) - f) + \overline{s_0}\dfrac{\partial P}{\partial t} + \nabla\cdot\left(\dfrac{\partial \mathbf{u}}{\partial t}\right)\right) g_{\mathcal{E}} = 0, & \text{(55f)}\\
\dfrac{\partial c}{\partial t} = \nabla\cdot(f\overline{\mathbf{D}^0_{\text{drug}}}\nabla c + cJ_{\text{drug}}) + c\left(-\dfrac{\overline{k^d_{\text{drug}}}}{f} - \nabla\cdot\left(\dfrac{\partial \mathbf{u}}{\partial t}\right)\right) + \dfrac{\alpha\mathcal{S}_{\text{drug}}}{c_0}. & \text{(55g)}
\end{cases}$$

Remark 4 (**Dynamics added on porosity's behavior**). In previous studies, the porosity of the medium (or volume fraction of fluid) is often regarded as a constant [10]. Models that include porosity changes [54] have used the following relation between $\nabla\cdot\mathbf{u}$ and φ_f:

$$f = \frac{f(0,\mathbf{x}) + \nabla\cdot\mathbf{u}}{1 + \nabla\cdot\mathbf{u}},$$

which is obtained traducing an hypothesis of infinitesimal displacement on the variation of volume, or more recently [68]

$$f = 1 - (1 - f(0,\mathbf{x}))e^{-\nabla\cdot\mathbf{u}},$$

which is obtained from Equation (55e) in the case of a biphasic system with only incompressible cells and incompressible fluid. However, in our case, since our main hypothesis is that the porosity is not only affected by the deformation of the medium but mostly by the ECM degradation

enzyme injected, we must derive an expression for the effective porosity directly from the mass balance laws of the ECM and cells constituents.
An expression for the effective volume fraction occupied by cells can be derived from the volume balance of the phase occupied by cells assuming the initial conditions $g_{\mathcal{C}}(0,\mathbf{x}) = g^0_{\mathcal{C}}(\mathbf{x})$ and $\nabla\cdot\mathbf{u}(0,\mathbf{x}) = 0$. Integrating Equation (55e),

$$g_{\mathcal{C}}(t,\mathbf{x}) = g^0_{\mathcal{C}}(\mathbf{x})e^{-\nabla\cdot\mathbf{u}-\overline{s_0}(P-P^0)}. \tag{56}$$

To obtain the effective volume fraction occupied by ECM, consider

$$\tilde{g}_{\mathcal{E}} = g_{\mathcal{E}}e^{\nabla\cdot\mathbf{u}+\overline{s_0}(P-P^0)}. \tag{57}$$

An equation for this quantity assuming the initial conditions $\nabla\cdot\mathbf{u}(0,\mathbf{x}) = 0$, $P(0,\mathbf{x}) = P^0(\mathbf{x})$ and $\tilde{g}_{\mathcal{E}}(0,\mathbf{x}) = g_{\mathcal{E}}(0,\mathbf{x}) = g^0_{\mathcal{E}}(\mathbf{x})$, is given by

$$\frac{\partial\tilde{g}_{\mathcal{E}}}{\partial t} + \left(\overline{K}h + \overline{a_r}(f(0,\mathbf{x}) - f)\right)\tilde{g}_{\mathcal{E}} = 0.$$

This equation reflects the fact that, regardless of the mechanical changes due to the displacement and the compressibility of the tissue, the ECM is deteriorated when in contact with the ECM degradation enzyme, but then reconstruct itself towards its initial state.

Figure 8: $\tilde{g}_{\mathcal{E}}$ is plotted versus time for an initial volume fraction of ECM of 0.3 and for different concentrations of enzyme applied continuously during 30 minutes, regardless of the space dependency. Both tendencies (degradation during injection - reconstruction) can easily be observed.

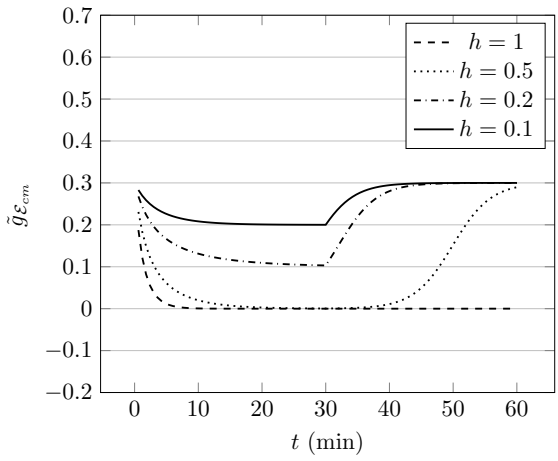

3.5 Boundary conditions

The primary variables of the problem are the displacement $\mathbf{u}$, the pressure P and the concentrations in ECM degradation enzyme h and in therapeutic agent c. Define the boundary of the domain Ω, denoted Γ. We generically denote by $\mathbf{n}$ the normal to Ω outwardly directed from the inside to the outside of the domain. Next, define the portions of the boundary Γ_u and Γ_t on which displacement and stress are defined, such as $\Gamma_u \cup \Gamma_t = \Gamma$ and

$$\mathbf{u} = \mathbf{u}_{\Gamma_u} \text{ on } \Gamma_u \text{ and } \mathbf{S}^E_s\,\mathbf{n} = \mathbf{t} \text{ on } \Gamma_t. \tag{58}$$

Applying the condition $\mathbf{S}^E_s\,\mathbf{n} = 0$ to the boundary amounts to considering a free boundary, while setting $\mathbf{u}_{\Gamma_u} = 0$ amounts to considering a fixed boundary.

The portions of the boundary Γ_p and Γ_q are the parts of the boundary on which pressure and pressure flux are specified, such as $\Gamma_p \cup \Gamma_q = \Gamma$ and

$$P = P_{\Gamma_p} \text{ on } \Gamma_p \text{ and } \nabla P \cdot \mathbf{n} = q \text{ on } \Gamma_q. \tag{59}$$

Setting a Dirichlet condition on the pressure amounts to considering a permeable boundary in contact with a surrounding medium where the pressure is fixed, while applying the condition $\nabla P \cdot \mathbf{n} = 0$ amounts to considering a wall boundary condition.
The portions of the boundary Γ_h and Γ_β are the parts of the boundary on which the enzyme's concentration and flux are specified, such as $\Gamma_h \cup \Gamma_\beta = \Gamma$ and

$$\begin{cases} h = h_{\Gamma_h} \text{ on } \Gamma_h, & \text{(60a)} \\ \left(f\mathbf{D}^0_{\text{enz}} \nabla h + h J_{\text{enz}}\right) \cdot \mathbf{n} = \beta_1 \text{ on } \Gamma_\beta. & \text{(60b)} \end{cases}$$

The same type of boundary conditions are applied to the therapeutic agent's concentration and flux

$$\begin{cases} c = c_{\Gamma_h} \text{ on } \Gamma_h, & \text{(61a)} \\ \left(f\mathbf{D}^0_{\text{drug}} \nabla c + c J_{\text{drug}}\right) \cdot \mathbf{n} = \beta_2 \text{ on } \Gamma_\beta. & \text{(61b)} \end{cases}$$

4 Numerical simulations

4.1 Computational algorithm

We first need to reduce the whole coupled system (55) to a sequence of linearized equations of simpler form. We subdivide the time interval $[0, T]$ into $N \geq 1$ uniform subintervals of length $\Delta t = \frac{T}{N}$, in such a way that the discrete time levels $t^n = n\Delta t$, $n = 0, \ldots, N$, are obtained. We set

$$\nabla \cdot \mathbf{u}^0 = 0, \quad g^0_{\mathcal{E}} = g_{\mathcal{E}}(0, \mathbf{x}), \quad \tilde{g}^0_{\mathcal{E}} = g_{\mathcal{E}}(0, \mathbf{x}), \quad g^0_{\mathcal{C}} = g_{\mathcal{C}}(0, \mathbf{x}), \quad h^0 = 0 \text{ and } c^0 = 0, \tag{62}$$

and P^0 is set as the solution of the steady-state pressure equation:

$$-\nabla \cdot (\overline{\boldsymbol{\kappa}}\, \nabla P^0) = \overline{\gamma}(\overline{p_v} - P^0), \tag{63}$$

coupled with the boundary conditions (59).
For $n = 0, \ldots, N-1$, we perform the following iteration:

1. We obtain f^n using (55a): $f^n = 1 - g^n_{\mathcal{E}} - g^n_{\mathcal{C}}$, and we set $g^n_s = g^n_{\mathcal{E}} + g^n_{\mathcal{C}}$.

2. We obtain $\mathbf{u}^{n+1}$ and P^{n+1} solving the linear poroelastic system with the finite element solver FreeFem++ [39], choosing P_2 (resp. P_1) elements for $\mathbf{u}^{n+1}$ (resp. P^{n+1}) to guarantee stable Galerkin approximation [32, 51] and discretizing in time with a first order backward Euler scheme [52]. Note that having a parabolic equation on P, which is a consequence of Assumption 3, numerically permits to prevent element locking [56].

$$\begin{cases} \nabla \cdot \left(g^n_s \left(\overline{\lambda}(\nabla \cdot \mathbf{u}^{n+1}) I + 2\overline{\mu}\boldsymbol{\varepsilon}(\mathbf{u}^{n+1})\right)\right) - \nabla P^{n+1} = 0, & \text{(64a)} \\ g^n_s \overline{s_0} \dfrac{P^{n+1}}{\Delta t} - \nabla \cdot (\overline{\boldsymbol{\kappa}}\, \nabla P^{n+1}) + \overline{\gamma} P^{n+1} + \dfrac{\nabla \cdot \mathbf{u}^{n+1}}{\Delta t} = g^n_s \overline{s_0} \dfrac{P^n}{\Delta t} + \dfrac{\nabla \cdot \mathbf{u}^n}{\Delta t} \\ \qquad + \alpha\, Q^{\text{tot}}_{\text{inj}}(t^{n+1}) + \overline{\gamma}\, \overline{p_{eq}} + \left(\dfrac{\rho^{R,0}_s}{\rho^R_f} - 1\right) g^n_{\mathcal{E}} (\overline{K} h^n + \overline{a_r}(f(0, \mathbf{x}) - f^n)), & \text{(64b)} \end{cases}$$

supplied by the approximation of the boundary conditions (58) and (59)

$$\begin{cases} \mathbf{u}^{n+1} = \mathbf{u}_{\Gamma_u} \text{ on } \Gamma_u \text{ and } \mathbf{S}_s^{E,n+1}\,\mathbf{n} = \mathbf{t} \text{ on } \Gamma_t, & \text{(65a)} \\ P^{n+1} = P_{\Gamma_p} \text{ on } \Gamma_p \text{ and } \nabla P^{n+1}\cdot\mathbf{n} = q \text{ on } \Gamma_q. & \text{(65b)} \end{cases}$$

3. Let us denote

$$J^n_{\text{enz}} = \frac{1}{f^n}\overline{\boldsymbol{\kappa}}\,\nabla P^n - \overline{\mathbf{D}^0_{\text{enz}}}\nabla f^n \qquad \text{and} \qquad J^n_{\text{drug}} = \frac{1}{f^n}\overline{\boldsymbol{\kappa}}\,\nabla P^n - \overline{\mathbf{D}^0_{\text{drug}}}\nabla f^n. \tag{66}$$

We obtain h^{n+1} and c^{n+1} solving the linear advection-diffusion-reaction equations still using the finite element solver FreeFem++ [39]

$$\frac{h^{n+1}}{\Delta t} - \nabla\cdot(f^n\overline{\mathbf{D}^0_{\text{enz}}}\nabla h^{n+1} + h^{n+1}J^n_{\text{enz}}) - h^{n+1}\left(-\frac{\overline{k^d_{\text{enz}}}}{f^n} - \left(\frac{\nabla\cdot\mathbf{u}^{n+1} - \nabla\cdot\mathbf{u}^n}{\Delta t}\right)\right) = \frac{h^n}{\Delta t} + \frac{\alpha}{c_0}\mathcal{S}_{\text{enz}}(t^{n+1}), \tag{67}$$

and

$$\frac{c^{n+1}}{\Delta t} - \nabla\cdot(f^n\overline{\mathbf{D}^0_{\text{drug}}}\nabla c^{n+1} + c^{n+1}J^n_{\text{drug}}) - c^{n+1}\left(-\frac{\overline{k^d_{\text{drug}}}}{f^n} - \left(\frac{\nabla\cdot\mathbf{u}^{n+1} - \nabla\cdot\mathbf{u}^n}{\Delta t}\right)\right) = \frac{c^n}{\Delta t} + \frac{\alpha}{c_0}\mathcal{S}_{\text{drug}}(t^{n+1}), \tag{68}$$

supplied by the following approximation of the boundary conditions (60) and (61):

$$\begin{cases} h^{n+1} = h_{\Gamma_h} \text{ on } \Gamma_h, \text{ and } \left(f^n\mathbf{D}^0_{\text{enz}}\nabla h^{n+1} + h^{n+1}J^n_{\text{enz}}\right)\cdot\mathbf{n} = \beta_1 \text{ on } \Gamma_\beta, & \text{(69a)} \\ c^{n+1} = h_{\Gamma_h} \text{ on } \Gamma_h, \text{ and } \left(f^n\mathbf{D}^0_{\text{drug}}\nabla c^{n+1} + c^{n+1}J^n_{\text{drug}}\right)\cdot\mathbf{n} = \beta_2 \text{ on } \Gamma_\beta. & \text{(69b)} \end{cases}$$

4. We obtain $g^{n+1}_{\mathcal{E}}$ by first calculating

$$\tilde{g}^{n+1}_{\mathcal{E}} = \frac{\tilde{g}^n_{\mathcal{E}}}{1 + \Delta t(\overline{K}h^{n+1} + \overline{a_r}(f(0,\mathbf{x}) - f^n))}.$$

and from (57), we deduce

$$g^{n+1}_{\mathcal{E}} = \tilde{g}^{n+1}_{\mathcal{E}} e^{-\nabla\cdot\mathbf{u}^{n+1} - \overline{s_0}(P^{n+1}-P^0)}.$$

To obtain $g^{n+1}_{\mathcal{C}}$, we use formula (56)

$$g^{n+1}_{\mathcal{C}} = g^0_{\mathcal{C}}(\mathbf{x}) e^{-\nabla\cdot\mathbf{u}^{n+1} - \overline{s_0}(P^{n+1}-P^0)}.$$

Remark 5 (**Triangulation convergence tests**). We checked numerically that the relative error e_h (resp. e_f, e_P) on the total mass of enzyme (resp. the quantity of fluid, the mean pressure) at $t = 60$ min decreases with order 1 when refining the mesh (Figure 9).

Remark 6 (**Conservation of mass**). A test case is performed to check if the total mass of enzyme injected is conserved when its degradation rate is zero. When the degradation rate is nonzero, the enzyme's total mass remains positive, and after reaching a maximum amount at the end of the injection, it decreases gradually till reaching zero as it has been observed in [53] (Figure 10).

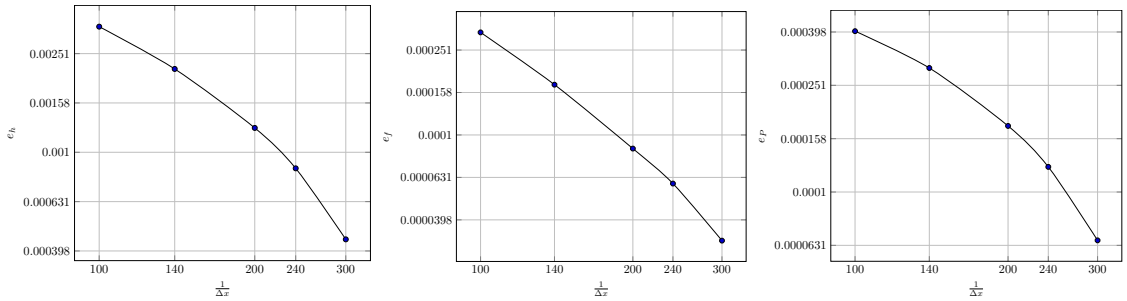

Figure 9: Results from the triangulation convergence simulations in 1D at $t = 60$ min (simulations from section 4.2). The relative error on $\int_\Omega Z(t = 60 \text{ min})\, dx$ with $Z = h$, f, P is plotted using logarithmic scales on both the horizontal and vertical axes.

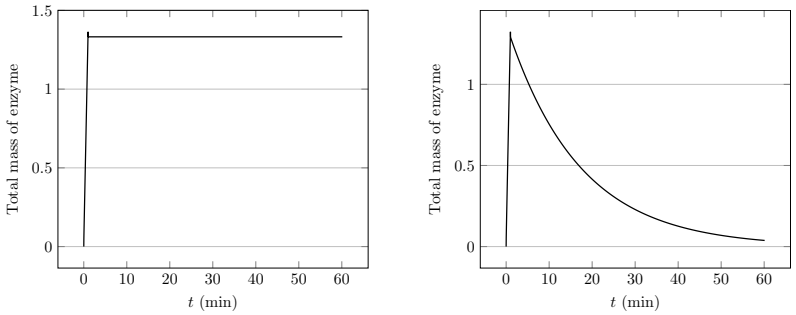

(a) Numerical mass conservation of enzyme.

(b) ECM degradation enzyme's total mass versus time when degradation rate is nonzero.

Figure 10: First numerical results on the total mass of enzyme. Numerically, the mass is well conserved when the degradation rate is zero, while the curve has the expected shape when the degradation rate is nonzero.

4.2 Numerical tests in 1D

The computational domain. In this section, we formulate the poroelastic transport model in a one-dimensional geometrical configuration (1D). Figure 11 shows a schematic representation of the 1D reference domain we considered. Denoting by x the spatial coordinate, the region $x < 0$ represents the tissue far away from the site of injection, the open interval $\Omega = (0, L)$ is the tissue whereas the region $x > L$ corresponds to the air surrounding the tissue.

Simulation Tests. What we want here is to understand the qualitative effect on the porosity of a injection of ECM degradation enzyme. Consequently, we consider in this section system (55) without equation (55g). In the simulations, $\overline{\gamma}$ is chosen so the initial pressure, derived from equation (63), is a constant.
To test the capability of the model, simulations are performed on the homogenous domain represented in Figure 11. The border of the domain is divided in two parts: $\Gamma = \Gamma_0 \cup \Gamma_f$. On Γ_0 ($x = 0$), Dirichlet boundary conditions are imposed, i.e. displacement $\mathbf{u}$ and concentration h are set to zero, and pressure P is set to $\overline{p_v}$. On Γ_f ($x = 1$), a free boundary condition is imposed

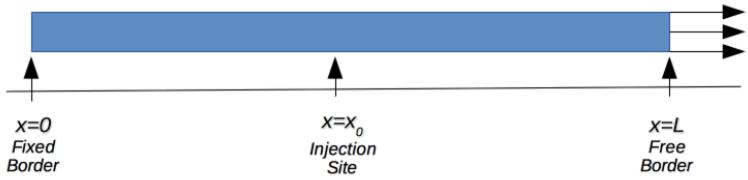

Figure 11: Schematic representation of the 1D reference domain.

on the displacement, i.e. $\mathbf{S}_s^E\mathbf{n} = 0$, while a wall condition is imposed on the pressure and the concentration h, i.e. $\nabla P \cdot \mathbf{n} = 0$ and $\left(\mathbf{D}^0_{\text{enz}}\nabla h + hJ_{\text{enz}}\right)\cdot\mathbf{n} = 0$. Visualization with the software FreeFem++ allows us to plot the porosity f and any other quantities of interest directly in a changing domain thanks to the function movemesh [39].
The principal scope of this serie of numerical experiments is to understand the qualitative behavior of the porosity after an injection of ECM degradation enzyme. Four sets of simulation tests are performed to investigate respectively the transport and effect of a passive substance (like water), the sole effect of degradation of the ECM by the enzyme injected, the effect of the enzyme on the ECM with recovery and the effect of the enzyme on the ECM with natural degradation of the enzyme. The fifth set of simulations corresponds to investigating how all the different effects interact together. Table 1 sums up these five different sets of simulations.

Table 1: Investigation of the effects on porosity of the parameters for each simulation test.

	K	a_r	k^d_{enz}	Considered Phenomena
Simulation 1	0	0	0	Passive transport
Simulation 2	0.5	0	0	Effect on ECM
Simulation 3	0.5	0.01	0	Effect on ECM + Recovery
Simulation 4	0.5	0	0.001	Effect on ECM + Natural degradation
Simulation 5	0.5	0.01	0.001	Effect on ECM + Recovery + Natural degradation

Simulations are performed first on the computational domain described in Figure 11 and the effects on the porosity f are investigated. Figures 12 represent the porosity of the medium at four different times for each simulation: after 1 minute, 10 minutes, 30 minutes and 1 hour.
In the case of passive transport of water, the porosity remains equal to its initial value (0.1 in all four simulations). In reality, the porosity varies a little bit because of the volume variation, but when plotted between 0 and 1 it is not obvious and it seems legitimate to assume that the porosity is a constant in this case (12a). In the second set of simulations, we want to investigate the sole effect of degradation of the ECM by the enzyme, without recovery of the tissue and without natural degradation of the enzyme. With $K = 0.01$, the effect of the enzyme on the ECM is immediate: after 1 minute, the ECM around the injection site has deteriorated. Then, with the diffusion of the enzyme, the area where the ECM deteriorates expands mostly towards the boundary Γ_f as the enzyme flows out the domain through boundary Γ_0, without ever overcrossing the maximum value possible $f + g_{\mathcal{E}} = 0.5$ (12b). When we add a recovery dynamic, we observe that at some point, the area where the ECM has deteriorated stops expanding and the porosity tends to get back to its initial state (12c). In the fourth set of simulations, the recovery dynamic is not considered anymore but we take into account the natural degradation of the enzyme. In this case, the area where the ECM deteriorates starts expanding then reaches its equilibrium

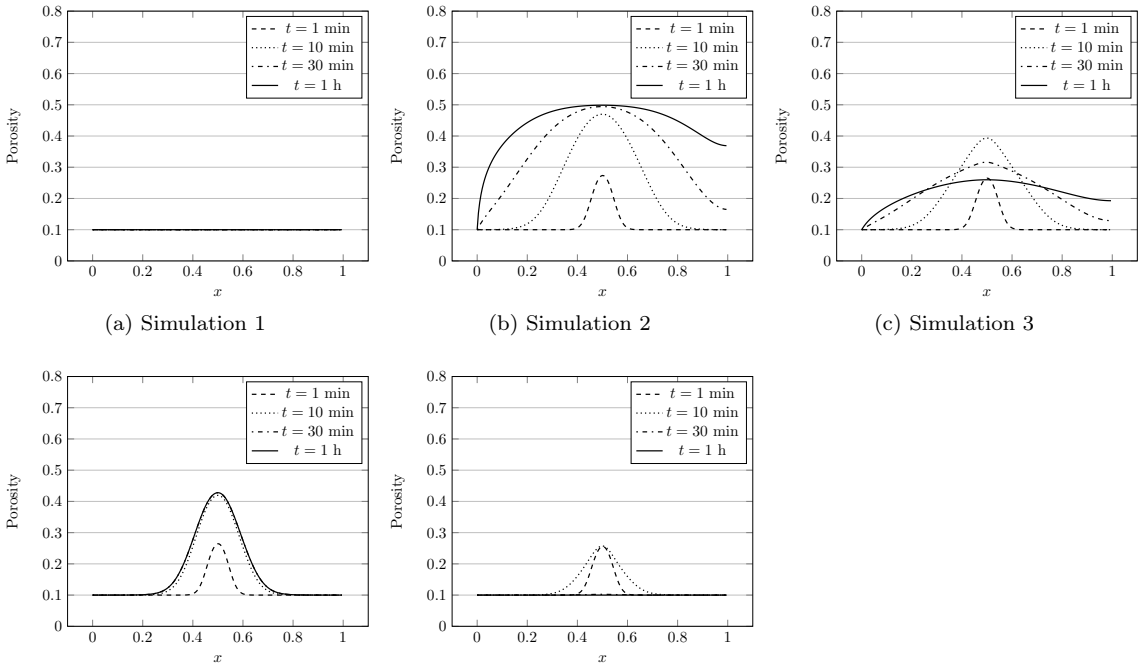

(a) Simulation 1 (b) Simulation 2 (c) Simulation 3

(d) Simulation 4 (e) Simulation 5

Figure 12: Porosity changes at $t = 1$ min, 10 min, 30 min and 1 hour in the 1D case.

state (12d). In the last set of simulations, all effects are considered together (12e).

4.3 Numerical tests in 2D

The computational domain. Figure 13 shows a schematic representation of the 2D reference domain we considered.

Figure 13: Schematic representation of the 2D reference domain. As in the 1D case, the border of the domain was divided in two parts: $\Gamma = \Gamma_0 \cup \Gamma_f$. On Γ_0, Dirichlet boundary conditions were imposed, while on Γ_f, free boundary conditions were imposed.

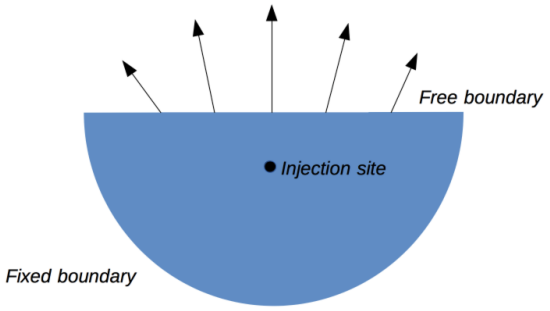

Simulation tests. As before, we consider in this section system (55) without equation (55g) and $\overline{\gamma}$ is chosen so the initial pressure, derived from equation (63), is a constant. Parameters K, a_r and k^d_{enz} are set in order to mainly observe during the simulation's time the deterioration effect of the enzyme on the ECM. This second set of simulation tests in 2D consists mainly in

comparing the isotropic and transverse isotropic cases. As expected the main difference lies in the shape of the area where the ECM has been deteriorated. These 2D simulations emphasize mainly the possibility offered by the mathematical model we developed of considering anisotropic media.

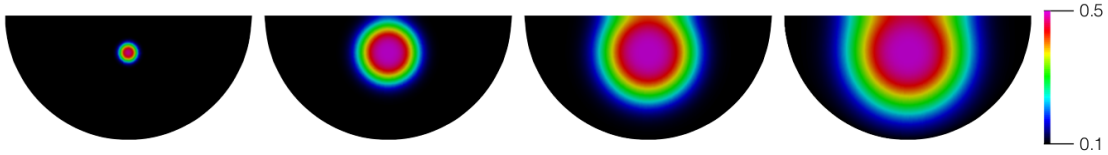

(a) Porosity at $t = 1, 10, 30, 60$ minutes in the 2D isotropic case

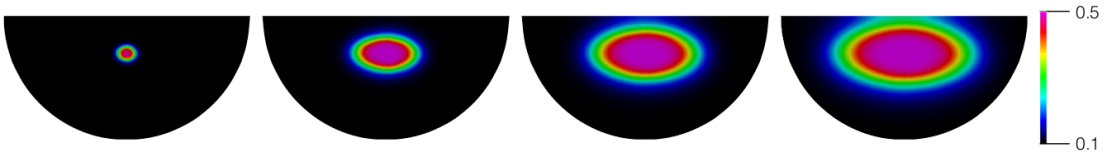

(b) Porosity at $t = 1, 20, 60, 120$ minutes in the 2D anisotropic case

Figure 14: Porosity changes at $t = 1$ min, 10 min, 30 min and 1 hour in the 2D case for $K = 50$, $a_r = 0.0005$ and $k^d_{\text{enz}} = 0.0001$.

5 Comparison with experiments: drug penetration in solid tumors

5.1 Experimental framework

To be most effective, anticancer drugs must penetrate tumor tissue efficiently, reaching all cells in a concentration suffcicient to exert a therapeutic effect. Nevertheless, the distribution of many anticancer drugs in tumor tissue is incomplete, as physiological transport barriers can strongly abate their efficiency [49, 71]. In particular, the composition and structure of the extracellular matrix can slow down the movement of molecules within the tumor [55]. Degradation of the ECM is assumed to improve the penetration of drugs. Delivery of drug to tumor cells occurs by two independent mechanisms: diffusion due to the concentration gradient and convection due to pressure gradient. It has been shown that both those mechanisms are enhanced when the tissue is previously injected or incubated with ECM degradation enzymes such as hyaluronidase and collagenase [29, 30, 28]. Multicellular spheroids are spherical aggregates of tumor cells that reflect many properties of solid tumors, including the development of an ECM, therefore they have been used to study the penetration of anticancer drugs into tumor tissue [49]. Experimental results are consistent in showing limited drug penetration into spheroids [69]. A pretreatment with hyaluronidase or collagenase was shown to increase the diffusion coefficient of larger molecules in spheroids, and the enzymatic treatment also improved the diffusion in the case of smaller molecules in tumor tissue [30], thereby improving the tissue's sensitivity to cytotoxic drugs [67, 43]. Spheroids models allow to evaluate the influence of diffusion on drugs transport, but some features of solid cancer such as variable IFP and the influence of convection (which commonly occurs in the periphery of tumors) are not modeled [49]. In vivo, the disorganized vascular network and the absence of functional lymphatics causes increased interstitial fluid pressure (IFP), which is uniformly elevated throughout a solid tumor and drops precipitously in the tumor

Table 2: Values of the model parameters in the simulations of Sections 4 and 5, except from K, a_r, k^d_{enz} otherwise specified. Parameters indexed with a * have different values in Section 5 (see Table 3).

Parameter	Symbol	Value	Unit	Reference
Typical lenght	l_0	10^{-2}	m	
Reference concentration	c_0	10^9	kg/m^3	
Density of fluid phase	ρ_f^R	10^3	kg/m^3	[76]
Density of solid phase	$\rho_s^{R,0}$	1.09×10^3	kg/m^3	[72]
Specific storage coefficient	s_0	10^{-6}	Pa^{-1}	
Injected concentration	$c^{\text{enz}}_{\text{inj}}$	4×10^{-2}	U/μl	[63]
Diffusion coefficient of the enzyme*	D^0_{enz}	10^{-8}	m^2/s	
Permeability	κ	10^{-11}	m^{2}Pa^{-1}s^{-1}	[70]
Lamé first parameter	λ	7.14×10^5	Pa	[77]
Lamé second parameter	μ	1.79×10^5	Pa	[77]
Diffusion coefficient perpendicular to a fiber's axis	$D^0_{\text{enz},\perp}$	10^{-8}	m^2/s	
Diffusion coefficient parallel to a fiber's axis	$D^0_{\text{enz},/\!/}$	$1.5 \times D^0_{\text{enz},\perp}$	-	[25]
Permeability perpendicular to a fiber's axis	$\kappa_\perp$	10^{-11}	m^{2}Pa^{-1}s^{-1}	
Permeability parallel to a fiber's axis	$\kappa_{/\!/}$	$1.5 \times \kappa_\perp$	-	
Elastic constants (TI case)	C_{1111}	2.64×10^6	Pa	[47]
	C_{1133}	3.39×10^6	Pa	[47]
	C_{1313}	10^2	Pa	[47]
	C_{3333}	4.4×10^6	Pa	[47]

Initial values	Symbol	Initial value	Unit
Volume fraction of fluid	$\varphi_f(0,\mathbf{x})$	0.1	-
Volume fraction of ECM	$\varphi_{\mathcal{E}}(0,\mathbf{x})$	0.4	-
Volume fraction of cells	$\varphi_{\mathcal{C}}(0,\mathbf{x})$	0.5	-
Network dilatation	$\nabla.\mathbf{u}(0,\mathbf{x})$	0	-
Concentration in enzyme	$h(0,\mathbf{x})$	0	Um^{-3}
Pressure	$p(0,\mathbf{x})$	0	Pa

periphery [40, 17]. The high IFP is a major obstacle to penetration of therapeutic molecules, as the transcapillary pressure gradient is low, and an outward interstitial flux is generated toward the periphery of the tumor due to the steep pressure gradient in the periphery of the tumor. It has been shown that hyaluronidase and collagenase reduce IFP, thereby improving the tumor uptake and distribution of molecules within solid tumors [29, 19]. The tumor (resp. spheroid) was modeled as a sphere and consequently we chose to perform numerical simulations in axisymmetry. We used the 2D computational domain shown in Figure 19. No calibration of the parameters was done, our objective being to observe the qualitative effects of the incubation with ECM degradation enzyme of a spheroid on diffusion on one hand, and of an intratumoral injection of ECM degradation enzyme on transcapillary transport on the other hand.

5.2 Effect of an ECM degradation enzyme on diffusion of therapeutic agent

5.2.1 Boundary conditions

Define the portions of the boundary Γ_{ext}, the surface of the spheroid, and Γ_{int} the inner boundaries. To take into account the axisymmetric geometry of the domain, we choose on the internal boundaries Γ_{int} homogeneous Neumann conditions on P, h and c and we impose that the displacement will only be radial. On the surface of a spheroid, there are no contact forces and the pressure at the outer edge is the same as the pressure in the surrounding medium, that we set to be equal to P_{ext}.

$$\begin{cases} \mathbf{S}_s^E \, \mathbf{n} = 0 \text{ on } \Gamma_{\text{ext}}, & \mathbf{u} \cdot \mathbf{n} = 0 \text{ on } \Gamma_{\text{int}}, \quad (70a) \\ P = P_{\text{ext}} \text{ on } \Gamma_{\text{ext}}, & \nabla P \cdot \mathbf{n} = 0 \text{ on } \Gamma_{\text{int}}, \quad (70b) \end{cases}$$

During the first hour, the spheroid is incubated with the enzyme, so instead of taking a source term in equation (55d), we choose a Dirichlet boundary condition on h.

$$\begin{cases} h = \dfrac{\alpha}{c_0} c_{\text{inj}}^{\text{enz}} \text{ on } \Gamma_{\text{ext}}, & \nabla h \cdot \mathbf{n} = 0 \text{ on } \Gamma_{\text{int}}, \end{cases} \quad (71)$$

After one hour, the medium containing the enzyme is removed and a fresh medium containing the molecule of interest is added. Consequently, we choose a Dirichlet boundary condition on c and we set the outter flux of enzyme to be zero.

$$\begin{cases} \left(\mathbf{D}_{\text{enz}}^0 \nabla h + h J_{\text{enz}}\right) \cdot \mathbf{n} = 0 \text{ on } \Gamma_{\text{ext}}, & \nabla h \cdot \mathbf{n} = 0 \text{ on } \Gamma_{\text{int}}, \quad (72a) \\ c = \dfrac{\alpha}{c_0} c_{\text{inj}}^{\text{drug}} \text{ on } \Gamma_{\text{ext}}, & \nabla c \cdot \mathbf{n} = 0 \text{ on } \Gamma_{\text{int}}. \quad (72b) \end{cases}$$

After a while, the spheroid can be removed from this second medium. In this third case, we set the outter flux of enzyme and of therapeutic agent to be zero.

$$\begin{cases} \left(\mathbf{D}_{\text{enz}}^0 \nabla h + h J_{\text{enz}}\right) \cdot \mathbf{n} = 0 \text{ on } \Gamma_{\text{ext}}, & \nabla h \cdot \mathbf{n} = 0 \text{ on } \Gamma_{\text{int}}, \quad (73a) \\ \left(\mathbf{D}_{\text{drug}}^0 \nabla c + c J_{\text{drug}}\right) \cdot \mathbf{n} = 0 \text{ on } \Gamma_{\text{ext}}, & \nabla c \cdot \mathbf{n} = 0 \text{ on } \Gamma_{\text{int}}. \quad (73b) \end{cases}$$

5.2.2 Effect on porosity

As expected, the porosity remains quasi constant and equal to its initial constant value (0.1 in this case) when the spheroid is incubated in a medium with no enzyme. On the contrary, it varies when the tissue is incubated with an ECM degradation enzyme. Thus, at $t = 60$ minutes, the ECM has been degraded substantially all over the spheroid, and although the degradation of the ECM is slightly higher at the boundary, the effect is quite homogeneous (Figure 15a). As far as the total mass of fluid within the spheroid is concerned, it increases gradually while the enzyme degrades the ECM (Figure 15b).

5.2.3 Results

ECM degradation enzymes such as collagenase and hyaluronidase where shown to increase the diffusion of macromolecules in spheroid and in tumor tissue, with a greater impact witnessed in the case of collagenase compared to hyaluronidase [30]. We performed simulations to evaluate the effect of an incubation of a spheroid with enzyme on the distribution of drugs with a low coefficient of diffusion ($D_{\text{drug}}^0 = 10^{-9}$ ui), such as the one of a macromolecule. We simulate

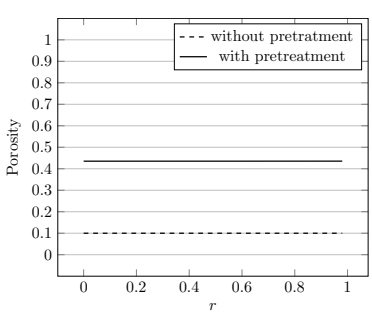

(a) Porosity versus radial position at the end of the incubation phase.

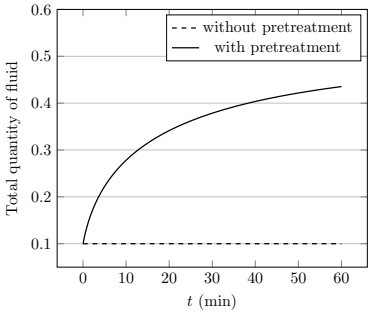

(b) Quantity of fluid in the tissue versus time.

Figure 15: Effect on the porosity of a tissue incubated with collagenase (20 U) during 60 minutes compared to incubated with a saline solution (0 U).

the incubation during 5 minutes with a therapeutic agent one hour after the incubation with collagenase and we observed the behavior of the drug's concentration for ten minutes, including the 5 minutes of incubation. It can be observed that the area where the drug is present above a certain minimum concentration is wider when the spheroid was previously incubated with collagenase (Figure 16).

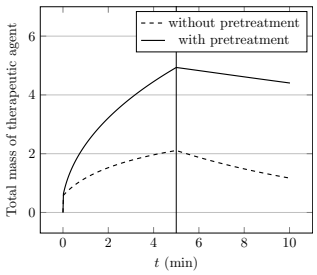

(a) Drug's total mass in the tissue versus time.

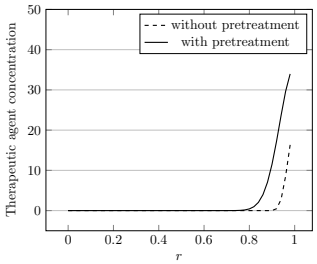

(b) Drug's concentration plotted versus the postion in the tumor at time $t = 10$ minutes.

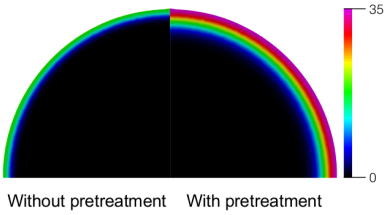

(c) 2D-drug's concentration in the tumor at time $t = 10$ minutes.

Figure 16: Numerical results for a therapeutic agent with a low coefficient of diffusion incubated during 5 minutes.

We then performed simulations to evaluate the effect of an incubation of a spheroid with enzyme on the distribution of drugs with an higher coefficient of diffusion ($D^0_{\text{drug}} = 10^{-6}$ ui), such as the one of a small molecule. In this case, the whole domain is affected with or without pretreatment, but the degraded ECM has two main effects: the drug reaches the whole domain faster, and naturally degrades slower which results in a higher concentration of drug throughout the tissue after 10 minutes (Figure 17).
We finally performed simulations with a quite low coefficient of diffusion ($D^0_{\text{drug}} = 10^{-8}$ ui), but for a tissue incubated longer (15 minutes) and we waited 15 more minutes to look at the drug's distribution. In this case, the result is qualitatively in agreement with the experiments developed by [43] (cf Figure 3): with an enzyme pretreatment, the drug distribution after 30 minutes (including 15 minutes of incubation) is way better than if the tissue was not pretreated

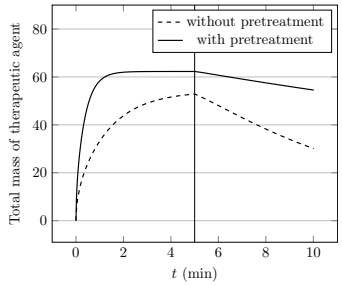

(a) Drug's total mass in the tissue versus time.

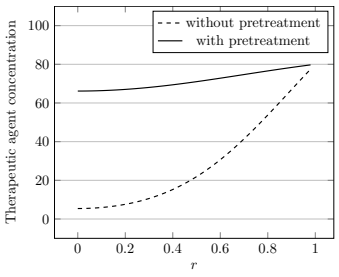

(b) Drug's concentration plotted versus the postion in the tumor at time $t = 1$ minute.

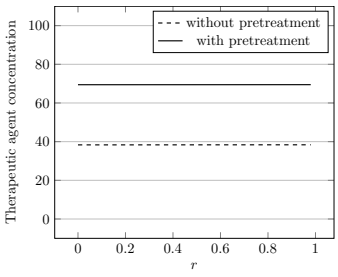

(c) Drug's concentration plotted versus the postion in the tumor at time $t = 10$ minutes.

Figure 17: Numerical results for a therapeutic agent with an higher coefficient of diffusion incubated during 5 minutes.

(Figure 18). The drug is not only present all over the tissue, its concentration is also higher, improving thus the chances of uptake by the cells.

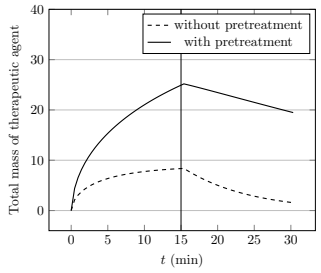

(a) Drug's total mass in the tissue versus time.

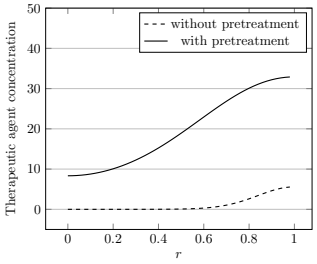

(b) Drug's concentration plotted versus the postion in the tumor at time $t = 30$ minutes.

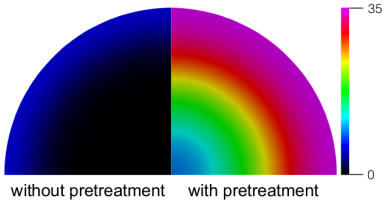

(c) 2D-drug's concentration in the tumor at time $t = 30$ minutes.

Figure 18: Numerical results for a therapeutic agent with a quite low coefficient of diffusion incubated during 15 minutes.

In the specific framework of an injection of DNA plasmids, a question of interest would be to determine when to do electrotransfer. If the best moment is when the area where the DNA plasmids concentration is above a certain minimum concentration is the widest, then the model, rightfully calibrated, could allow to calculate this optimized time.

5.3 Effect of an ECM degradation enzyme on transcapillary transport of therapeutic agent

5.3.1 Boundary conditions

Define the portions of the boundary Γ_{ext}, the surface of the tumor, and Γ_{int} the inner boundaries. On the surface of an isolated tumor, there are no contact forces and the pressure at the outer edge is the same as the pressure in the surrounding tissue, that we set to zero. On the concentration of the injected species, we assume that their flux is zero on Γ_{ext}. To take into account the axisymmetric geometry of the domain, we choose on the internal boundaries Γ_{int} homogeneous

Table 3: Values of the specific model parameters in the simulations of Section 5. All other parameters are taken from Table 2.

Parameter	Symbol	Value	Unit	Reference
Diffusion coefficient of the enzyme	D^0_{enz}	10^{-4}	m^2/s	
Diffusion coefficient of the therapeutic agent	D^0_{drug}	10^{-9}, 10^{-6}, 10^{-8}	m^2/s	
Starling's coefficient	γ	5×10^{-5}	$\text{Pa}^{-1}\text{s}^{-1}$	[64]
Fluid/solute coefficient	γ_c	0.9	-	[13]
Measure of treatment efficacity	K	10^{-14}	$\text{m}^3\text{s}^{-1}\text{U}^{-1}$	
Recovery coefficient	a_r	5×10^{-4}	s^{-1}	
Degradation rate of the enzyme	k^d_{enz}	1×10^{-4}	s^{-1}	
Degradation rate of the therapeutic agent	k^d_{drug}	2×10^{-4}	s^{-1}	
Driving pressure	P_v	10^{-1}	Pa	

Initial values	Symbol	Initial value	Unit
Concentration in drug	$c(0, \mathbf{x})$	0	kg m^{-3}
Pressure incubation case	$p(0, \mathbf{x})$	0	Pa

Neumann conditions on P, h and c and we impose that the displacement will only be radial.

$$\begin{cases} \mathbf{S}_s^E \, \mathbf{n} = 0 \text{ on } \Gamma_{\text{ext}}, & \mathbf{u} \cdot \mathbf{n} = 0 \text{ on } \Gamma_{\text{int}}, \quad (74a) \\ P = 0 \text{ on } \Gamma_{\text{ext}}, & \nabla P \cdot \mathbf{n} = 0 \text{ on } \Gamma_{\text{int}}, \quad (74b) \\ \left(\mathbf{D}^0_{\text{enz}} \nabla h + h J_{\text{enz}}\right) \cdot \mathbf{n} = 0 \text{ on } \Gamma_{\text{ext}}, & \nabla h \cdot \mathbf{n} = 0 \text{ on } \Gamma_{\text{int}}, \quad (74c) \\ \left(\mathbf{D}^0_{\text{drug}} \nabla c + c J_{\text{drug}}\right) \cdot \mathbf{n} = 0 \text{ on } \Gamma_{\text{ext}}, & \nabla c \cdot \mathbf{n} = 0 \text{ on } \Gamma_{\text{int}}. \quad (74d) \end{cases}$$

5.3.2 Initial pressure profile

In the simulations, $\overline{P_v}$ and $\overline{\gamma}$ are chosen so the initial pressure profile, derived from equation (63), fits the type of IFP profile observed in tumors (Figure 19).

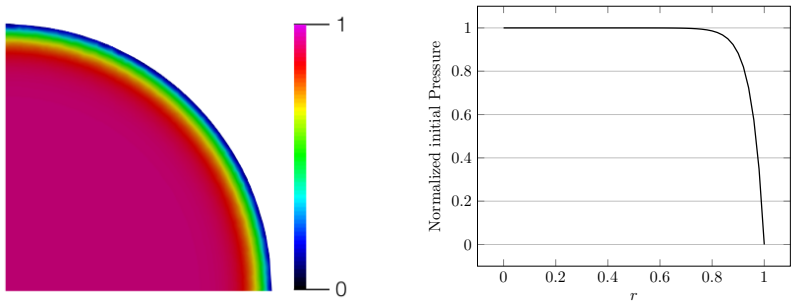

(a) Normalized 2D-pressure in the tumor before the experiment.

(b) Normalized pressure in the tumor before the experiment versus position.

Figure 19: Initial normalized pressure profile. This type of steep profile is in agreement with previous studies [13].

5.3.3 Effect on porosity

As it was previously observed in Section 4.2, the porosity remains quasi constant when only a saline solution is injected. On the contrary, it varies when the tissue is injected with an ECM degradation enzyme. At $t = 60$ minutes, we observe that without enzyme, the porosity is equal to its initial constant value (0.1 in this case) while in presence of enzyme, the ECM has been degraded substantially all over the tissue. Although the degradation of the ECM is the slightly higher in the vicinity of the injection point, the effect is quite homogeneous. As expected, the total mass of fluid within the tissue increases gradually while the enzyme degrades the ECM.

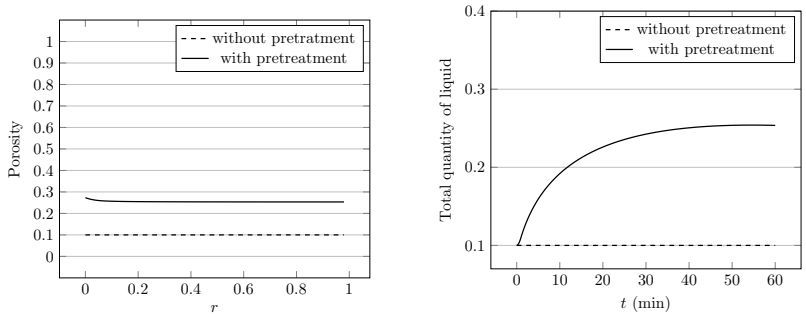

(a) Porosity versus radial position 60 minutes after the injection.

(b) Quantity of fluid in the tissue versus time.

Figure 20: Effect on the porosity of a tumor injected with hyaluronidase (1500 U) compared to injected with a saline solution (0 U).

5.3.4 Effect on the IFP

The effect of hyaluronidase on IFP was demonstrated experimentally by [29] and [19]. Intratumoral injection of hyaluronidase in tumors reduced IFP in a dose-dependent manner up to a maximum reduction. However, by increasing the dose further, IFP was reduced to a lesser extent. An initial increase in IFP was observed, explained by the increase in the volume and compression of the tissue at the moment of the intratumoral injection.
The simulation reproduces the three main effects observed in the experiments: an initial increase in IFP due to the intratumoral injection, the fact that IFP reaches a reduced value after some time and finally the non-linear behavior regarding the concentration.

5.3.5 Results

It was shown that both hyaluronidase and collagenase increase convection by inducing transcapillary pressure gradients in human osteosarcoma xenografts [29, 28]. We have seen previously that an injection of enzyme has an effect on the IFP, inducing a transcapillary pressure gradient in a dose-dependent manner up to a maximum reduction. Increasing the dose further, IFP is reduced to a lesser extent. This reduction was shown to improve both the distribution and the uptake of drugs in tumors [29]. In this section, we focus on the distribution of drugs. We simulate an injection during 1 minute of a therapeutic agent one hour after the injection of enzyme and we observed the behavior of the drug's concentration for ten minutes, including during the injection. For all simulatiojns, the same value of $c_v(t, \mathbf{x}) = \chi_{\{0 \leq t \leq 1\,\mathrm{min}\}}(t)\, c_v$ is taken while different values of $c_{\mathrm{inj}}^{\mathrm{enz}}$ previously injected are considered. For a drug with a low coefficient of diffusion, such as

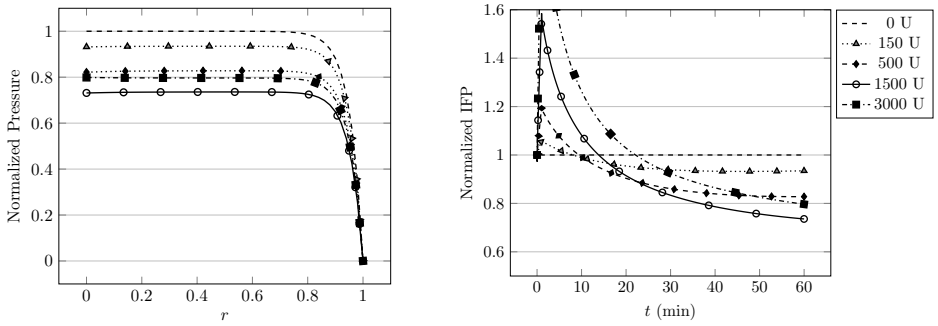

(a) Normalized IFP versus position at time $t = 60$ minutes.

(b) Normalized IFP versus time.

Figure 21: Effect on the normalized interstitial fluid pressure of a tumor injected with hyaluronidase (500 U, 1500 U, 3000 U) compared to injected with a saline solution.

the one of a macromolecule, several features are observed. First, the total mass of therapeutic agent that actually reaches the tumor by transcapillary transport varies with the concentration of enzyme previously injected (Figure 22a). Second, while without enzyme the therapeutic agent only penetrates the periphery of the tumor, we observe that with a pretreatment, the therapeutic agent is present all over the tumor (Figure 22b). Finally, the same non-linear behavior regarding the concentration of enzyme previously injected is observed. In particular, if the concentration of enzyme is too high, as the pressure is reduced to a lesser extent, the drug's penetration in the tumor by transcapillary transport is also reduced.

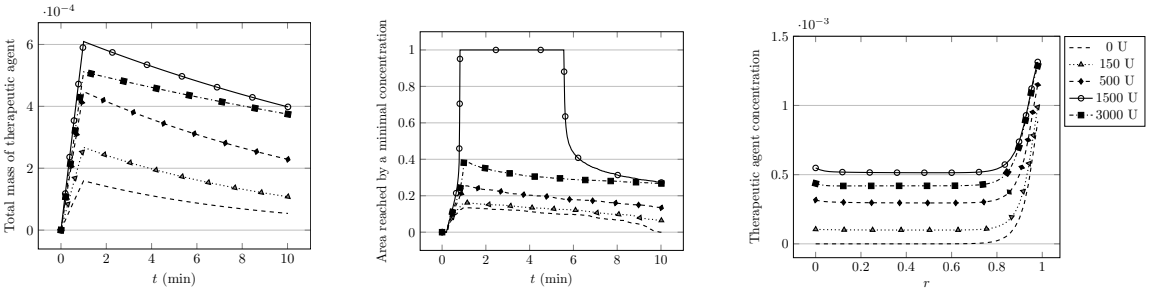

(a) Drug's total mass in the tissue versus time.

(b) Normalized area reached by a minimal concentration of therapeutic agent versus time.

(c) Drug's concentration plotted versus the postion in the tumor at time $t = 5$ minutes.

Figure 22: Numerical results for a therapeutic agent with a low coefficient of diffusion injected intravenously.

For a drug with an higher coefficient of diffusion, such as the one of a smaller molecule, the transcapillary transport in the tumor is also improved, but the main features of interest are different. In particular, as the drug reaches the whole tumor mainly by diffusion in any case, the contributions of the pretreatment of the tumor with an ECM degradation enzyme are the same as the ones developed in the previous subsection concerning spheroids. In particular, it is when the concentration of enzyme previously injected is the highest that the drug reaches homogeneously the tumor the fastest and that the natural degradation process is slowed the most. Nevertheless,

the total mass of therapeutic agent that actually reaches the tumor by transcapillary transport is consistent with the reduction of IFP in the same non-linear behavior regarding the concentration of enzyme, and consequently, at $t = 10$ minutes, the best configuration is also obtained for the concentration of enzyme that induces the highest reduction in IFP.

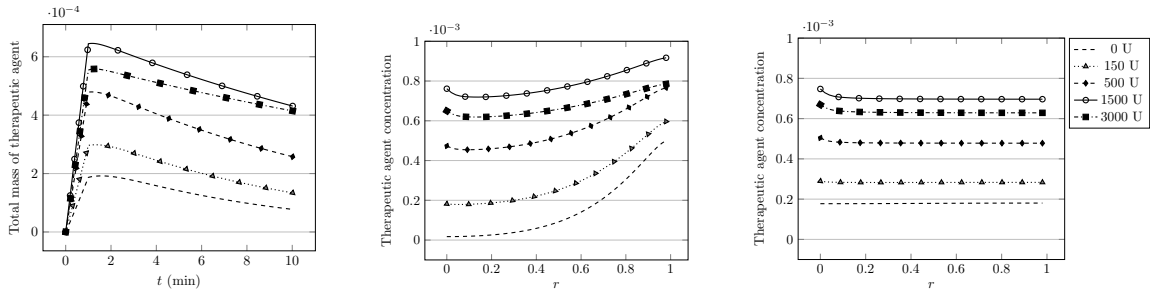

(a) Drug's total mass in the tissue versus time.

(b) Drug's concentration plotted versus the postion in the tumor at time $t = 1$ minute.

(c) Drug's concentration plotted versus the postion in the tumor at time $t = 5$ minutes.

Figure 23: Numerical results for a therapeutic agent with an higher coefficient of diffusion injected intravenously.

The distribution of the drug into the tissue is directly correlated with the transcapillary pressure gradient created by the hyaluronidase injected. In particular, it is for the hyaluronidase's concentration value for which the maximum pressure reduction is obtained that we obtained the best distribution profile. Increasing the dose further, the pressure is reduced to a lesser extent and the consequence on the distribution of drug is that the area where the concentration of therapeutic agent is above a minimum concentration value is smaller. This result is in agreement with the experiments described by [29] where hyaluronidase was shown to improve the distribution of doxorubicin considerably. To go further and consider the possibility of using the model as a strategie to optimize drug delivery, we would need more experimental data to calibrate the model parameters.

6 Conclusion

In this paper we developed a novel mathematical formulation to describe the effect of an ECM degradation enzyme on a soft biological tissue. The principal novelty of our contribution is the development of a model based on the use of Partial Differential Equations (PDEs) that incorporates the effect of an ECM degradation enzyme within the general and well established framework of poroelastic theory of mixtures. Specifically, where usually the fraction volumes of the different phases are assumed to be constants, we derive evolutive equations to describe them. Having defined the possible interactions between phases, our approach consists in deriving a system of conservation laws (mass and linear momentum) for the phases and components of the mixture that includes the enzyme's concentration as main determinant of porosity evolution. The next step was to develop a numerical approximation of the mathematical model introduced in the article. As the medium is assumed to be poroelastic, it can undergo some deformation and potentially change of shape if a boundary condition is applied on stress. It was necessary to formulate our model in a reference fixed domain before developing a computational algorithm to approximate the system's solution. Below we address the more significant outcomes of the conducted simulations.

1. The illustrated numerical tests conducted in 1D indicate the role of each new parameter on the porosity evolution.

2. The illustrated numerical results in 2D can describe a well known principle of prefential flow in the direction of the fiber tracts in the context of a transverse anisotropic media.

3. Model simulations indicate that an intratumoral injection of hyaluronidase results in a reduction of the IFP in a dose-dependent manner up to a maximum reduction, and that once that maximum reduction is achieved, a further increase of the dose results in a smaller reduction. This finding represents a favorable result from the experimentalist point of view, because it is in agreement with several observations previously reported.

4. The injection of an ECM degradation enzyme was also shown to enhance distribution, by improving diffusion and/or convection, of drug throughout the tissue. This outcome reinforces the idea that, used in medicine, these enzymes can improve a treatment by widening its field of action.

Further research effort will be devoted to calibrating the model's parameters with additional experimental data and to considering domains with more complex 3D geometries. An effort will also be made to rightfully coupled this model with an electrical model in order to explain and quantify the uptake of DNA plasmids observed by [63].

Acknowledgements. M.D. is partly granted by "Université Franco-Italienne", project VINCI C2-25. M.D. and C.P. are partly granted by the Plan Cancer DYNAMO (Inserm 9749) and Plan Cancer NUMEP (Inserm 11099). This study has been carried out within the scope of the European Associate Lab EBAM, and the Inria Associate Team Num4SEP.

References

[1] T. Akerstrom, K. Vedel, J. Needham, and P. Hojman. Optimizing hyaluronidase dose and plasmid DNA delivery greatly improves gene electrotransfer efficiency in rat skeletal muscle. *Biochemistry and Biophysics Reports*, 2015.

[2] G. Alì, V. Furuholt, R. Natalini, and I. Torcicollo. A mathematical model of sulphite chemical aggression of limestones with high permeability. Part I. Modeling and qualitative analysis. *Transport in Porous Media*, 69:109–122, 2007.

[3] P. M. Altrock, L. L. Liu, and F. Michor. The mathematics of cancer: integrating quantitative models. *Nature Reviews Cancer*, 15(12):730–745, Dec. 2015.

[4] D. Ambrosi. Infiltration through deformable porous media. *ZAMM. Zeitschrift für Angewandte Mathematik und Mechanik. Journal of Applied Mathematics and Mechanics*, 82(2):115–124, 2002.

[5] F. André and L. M. Mir. DNA electrotransfer: its principles and an updated review of its therapeutic applications. *Gene therapy*, 11 Suppl 1:S33–42, Oct. 2004.

[6] S. Astanin and L. Preziosi. *Selected Topics in Cancer Modeling: Genesis, Evolution, Immune Competition, and Therapy*, chapter Multiphase Models of Tumour Growth, pages 1–31. Birkhäuser Boston, 2008.

[7] Y. H. Bae, R. J. Mrsny, and K. Park. Cancer targeted drug delivery, 2013.

[8] S. I. Barry and G. K. ALDIS. Unsteady-Flow Induced Deformation of Porous Materials. *International Journal of Non-Linear Mechanics*, 26(5):687–699, 1991.

[9] S. I. Barry and G. N. Mercer. Flow and deformation in poroelasticity. I. Unusual exact solutions. *Mathematical and Computer Modelling*, 30(9-10):23–29, 1999.

[10] P. J. Basser. Interstitial pressure, volume, and flow during infusion into brain tissue. *Microvascular research*, 44(2):143–165, Sept. 1992.

[11] R. C. Batra. Linear constitutive relations in isotropic finite elasticity. *Journal of Elasticity. The Physical and Mathematical Science of Solids*, 51(3):243–245, 1998.

[12] G. Baumgartner. The impact of extracellular matrix on chemoresistance of solid tumors–experimental and clinical results of hyaluronidase as additive to cytostatic chemotherapy. *Cancer letters*, 131(1):1–2, Sept. 1998.

[13] L. T. Baxter and R. K. Jain. Transport of fluid and macromolecules in tumors. I. Role of interstitial pressure and convection. *Microvascular research*, 1989.

[14] J. Bear and Y. Bachmat. *Introduction to Modeling of Transport Phenomena in Porous Media*. Kluwer Academic Publishers, 1990.

[15] M. A. Biot. General theory of three-dimensional consolidation. *Journal of applied physics*, 12(2):155, 1941.

[16] A. Bottaro and T. Ansaldi. On the infusion of a therapeutic agent into a solid tumor modeled as a poroelastic medium. *Journal of biomechanical engineering*, 134(8):084501, Aug. 2012.

[17] Y. Boucher, L. T. Baxter, and R. K. Jain. Interstitial Pressure Gradients in Tissue-isolated and Subcutaneous Tumors: Implications for Therapy. *Cancer research*, 50(15):4478–4484, Aug. 1990.

[18] R. M. Bowen. Incompressible porous media models by use of the theory of mixtures. *International Journal of Engineering Science*, 18(9):1129–1148, Jan. 1980.

[19] C. Brekken and C. de Lange Davies. Hyaluronidase reduces the interstitial fluid pressure in solid tumours in a non-linear concentration-dependent manner. *Cancer letters*, 131(1):65–70, Sept. 1998.

[20] B. A. Buhren, H. Schrumpf, N.-P. Hoff, E. Bölke, S. Hilton, and P. A. Gerber. Hyaluronidase: from clinical applications to molecular and cellular mechanisms. *European journal of medical research*, 21(1):5, 2016.

[21] M. F. Bureau, S. Naimi, R. T. Ibad, and J. Seguin. Intramuscular plasmid DNA electrotransfer: biodistribution and degradation. *Biochimica et Biophysica Acta (BBA)*, 2004.

[22] M. A. J. Chaplain, L. Graziano, and L. Preziosi. Mathematical modelling of the loss of tissue compression responsiveness and its role in solid tumour development. *Mathematical medicine and biology : a journal of the IMA*, 23(3):197–229, Sept. 2006.

[23] Z. Chen, G. Huan, and Y. Ma. *Computational methods for multiphase flows in porous media*. Computational Science & Engineering. Society for Industrial and Applied Mathematics (SIAM), Philadelphia, PA, 2006.

[24] I.-K. Choi, R. Strauss, M. Richter, C.-O. Yun, and A. Lieber. Strategies to increase drug penetration in solid tumors. *Frontiers in oncology*, 3:193, 2013.

[25] G. G. Cleveland, D. C. Chang, C. F. Hazlewood, and H. E. Rorschach. Nuclear magnetic resonance measurement of skeletal muscle: anisotrophy of the diffusion coefficient of the intracellular water. *Biophysical journal*, 16(9):1043–1053, Sept. 1976.

[26] B. M. Damon, A. Buck, and Z. Ding. Diffusion-tensor mri-based skeletal muscle fiber tracking. *Imaging in medicine*, 2011.

[27] H. Delingette. Toward realistic soft-tissue modeling in medical simulation. In *Proceedings of the IEEE*, 1998.

[28] L. Eikenes, Ø. S. Bruland, C. Brekken, and C. d. L. Davies. Collagenase increases the transcapillary pressure gradient and improves the uptake and distribution of monoclonal antibodies in human osteosarcoma xenografts. *Cancer research*, 64(14):4768–4773, July 2004.

[29] L. Eikenes, M. Tari, I. Tufto, Ø. S. Bruland, and C. de Lange Davies. Hyaluronidase induces a transcapillary pressure gradient and improves the distribution and uptake of liposomal doxorubicin (Caelyx) in human osteosarcoma xenografts. *British journal of cancer*, 93(1):81–88, July 2005.

[30] L. Eikenes, I. Tufto, E. A. Schnell, A. Bjørkøy, and C. De Lange Davies. Effect of collagenase and hyaluronidase on free and anomalous diffusion in multicellular spheroids and xenografts. *Anticancer research*, 30(2):359–368, Feb. 2010.

[31] J.-M. Escoffre, J. Teissie, and M.-P. Rols. Gene transfer: how can the biological barriers be overcome? *The Journal of membrane biology*, 236(1):61–74, July 2010.

[32] X. Feng, Z. Ge, and Y. Li. Multiphysics Finite Element Methods for a Poroelasticity Model. *arXiv.org*, Nov. 2014.

[33] C. Frantz, K. M. Stewart, and V. M. Weaver. The extracellular matrix at a glance. *Journal of cell science*, 123(Pt 24):4195–4200, Dec. 2010.

[34] Y. C. Fung. Biomechanics: mechanical properties of living tissues, 1981.

[35] L. Fusi, A. Farina, and D. Ambrosi. Mathematical Modeling of a Solid–Liquid Mixture with Mass Exchange Between Constituents. *Mathematics and Mechanics of Solids*, 11(6):575–595, Dec. 2006.

[36] S. Ganesh, M. Gonzalez-Edick, D. Gibbons, M. Van Roey, and K. Jooss. Intratumoral coadministration of hyaluronidase enzyme and oncolytic adenoviruses enhances virus potency in metastatic tumor models. *Clinical cancer research : an official journal of the American Association for Cancer Research*, 14(12):3933–3941, June 2008.

[37] K. S. Girish and K. Kemparaju. The magic glue hyaluronan and its eraser hyaluronidase: a biological overview. *Life sciences*, 80(21):1921–1943, May 2007.

[38] M. F. K. Happel, H. Niekisch, L. L. Castiblanco Rivera, F. W. Ohl, M. Deliano, and R. Frischknecht. Enhanced cognitive flexibility in reversal learning induced by removal of the extracellular matrix in auditory cortex. *Proceedings of the National Academy of Sciences of the United States of America*, 111(7):2800–2805, Feb. 2014.

[39] F. Hecht. New development in FreeFem++. *Journal of numerical mathematics*, 2012.

[40] R. K. Jain and L. T. Baxter. Mechanisms of Heterogeneous Distribution of Monoclonal Antibodies and Other Macromolecules in Tumors: Significance of Elevated Interstitial Pressure. *Cancer research*, 48(24 Part 1):7022–7032, Dec. 1988.

[41] L. Juhlin. Reconstitution of dermal connective tissue barrier after testicular or bacterial hyaluronidase. *Acta Pharmacologica et Toxicologica*, 12(1):96–108, 1956.

[42] R. Juliano. Challenges to macromolecular drug delivery. *Biochemical Society transactions*, 35(Pt 1):41–43, Feb. 2007.

[43] N. Kohno, T. Ohnuma, and P. Truog. Effects of hyaluronidase on doxorubicin penetration into squamous carcinoma multicellular tumor spheroids and its cell lethality. *Journal of cancer research and clinical oncology*, 120(5):293–297, 1994.

[44] G. E. Lang, D. Vella, S. L. Waters, and A. Goriely. Mathematical modelling of blood-brain barrier failure and oedema. *Mathematical medicine and biology : a journal of the IMA*, June 2016.

[45] C. Lelli, R. Sacco, P. Causin, and M. T. Raimondi. A poroelastic model of mechanobiological processes in tissue engieering. part i : Mathematical formulation. *doi: arXiv:1512.02182 (2015). Under review in Journal of Mathematical Biology*, 2015.

[46] G. Lemon, J. R. King, H. M. Byrne, O. E. Jensen, and K. M. Shakesheff. Mathematical modelling of engineered tissue growth using a multiphase porous flow mixture theory. *Journal of Mathematical Biology*, 52(5):571–594, May 2006.

[47] S. F. Levinson. Ultrasound propagation in anisotropic soft tissues: the application of linear elastic theory. *Journal of biomechanics*, 20(3):251–260, 1987.

[48] M. Magzoub, S. Jin, and A. S. Verkman. Enhanced macromolecule diffusion deep in tumors after enzymatic digestion of extracellular matrix collagen and its associated proteoglycan decorin. *FASEB journal : official publication of the Federation of American Societies for Experimental Biology*, 22(1):276–284, Jan. 2008.

[49] A. I. Minchinton and I. F. Tannock. Drug penetration in solid tumours. *Nature Reviews Cancer*, 2006.

[50] V. C. Mow, M. H. Holmes, and W. M. Lai. Fluid transport and mechanical properties of articular cartilage: a review. *Journal of biomechanics*, 17(5):377–394, 1984.

[51] M. A. Murad and A. F. D. Loula. Improved accuracy in finite element analysis of Biot's consolidation problem. *Computer Methods in Applied Mechanics and Engineering*, 95(3):359–382, 1992.

[52] M. A. Murad and A. F. D. Loula. On stability and convergence of finite element approximations of Biot's consolidation problem. *International Journal for Numerical Methods in Engineering*, 37(4):645–667, 1994.

[53] H. Namazi, V. V. Kulish, A. Wong, and S. Nazeri. Mathematical Based Calculation of Drug Penetration Depth in Solid Tumors. *BioMed research international*, 2016:8437247, 2016.

[54] P. A. Netti, L. T. Baxter, Y. Boucher, R. Skalak, and R. K. Jain. Macro- and microscopic fluid transport in living tissues: Application to solid tumors. *AIChE Journal*, 43(3):818–834, Mar. 1997.

[55] P. A. Netti, D. A. Berk, M. A. Swartz, A. J. Grodzinsky, and R. K. Jain. Role of extracellular matrix assembly in interstitial transport in solid tumors. *Cancer research*, 60(9):2497–2503, May 2000.

[56] P. J. Phillips and M. F. Wheeler. Overcoming the problem of locking in linear elasticity and poroelasticity: an heuristic approach. *Computational Geosciences*, 2009.

[57] L. Preziosi and A. Tosin. Multiphase modelling of tumour growth and extracellular matrix interaction: mathematical tools and applications. *Journal of Mathematical Biology*, 58(4-5):625–656, Oct. 2008.

[58] F. A. Radu, I. S. Pop, A. Muntean, and I. Berre. Simulation of reactive flow in porous media with variable porosity as appears when modelling concrete carbonation. In *11th World Congress on Computational Mechanics (WCCM XI), 5th European Conference on Computational Mechanics (ECCM V), 6th European Conference on Computational Fluid Dynamics (ECFD VI)*, Barcelona, Spain, 2014.

[59] J. Rosler, H. Harders, and M. Baker. Mechanical behaviour of engineering materials, 2007.

[60] D. Royer, J.-L. Gennisson, T. Deffieux, and M. Tanter. On the elasticity of transverse isotropic soft tissues (L). *The Journal of the Acoustical Society of America*, 129(5):2757–5, 2011.

[61] J. D. Schertzer, D. R. Plant, and G. S. Lynch. Optimizing plasmid-based gene transfer for investigating skeletal muscle structure and function. *Molecular Therapy*, 13(4), 2006.

[62] D. Signori, R. Lancellotta, and L. Preziosi. Mathematical models for soil consolidation problems : a state of the art report. *Chapter 6 of Modeling and Mechanics of Granular and Porous Materials*, pages 159–180, 2002.

[63] E. Signori, K. Wells, V. Fazio, and D. Wells. Optimisation of electrotransfer of plasmid into skeletal muscle by pretreatment with hyaluronidase - increased expression with reduced muscle damage. *Gene Therapy*, 8:1264–1270, 2001.

[64] M. Soltani and P. Chen. Effect of tumor shape and size on drug delivery to solid tumors. *Journal of biological engineering*, 2012.

[65] M. Spiegelman. Flow in deformable porous media. Part 1 Simple analysis. *Journal of Fluid Mechanics*, 247(-1):17–38, Feb. 1993.

[66] M. Spiegelman. Flow in deformable porous media. Part 2 Numerical analysis – the relationship between shock waves and solitary waves. *Journal of Fluid Mechanics*, 247(-1):39–63, Feb. 1993.

[67] B. St Croix, S. Man, and R. S. Kerbel. Reversal of intrinsic and acquired forms of drug resistance by hyaluronidase treatment of solid tumors. *Cancer letters*, 131(1):35–44, Sept. 1998.

[68] K. H. Støverud, M. Darcis, R. Helmig, and S. M. Hassanizadeh. Modeling Concentration Distribution and Deformation During Convection-Enhanced Drug Delivery into Brain Tissue. *Transport in Porous Media*, 92(1):119–143, Oct. 2011.

[69] R. M. Sutherland, H. A. Eddy, B. Bareham, K. Reich, and D. Vanantwerp. Resistance to adriamycin in multicellular spheroids. *International journal of radiation oncology, biology, physics*, 5(8):1225–1230, Aug. 1979.

[70] M. A. Swartz and M. E. Fleury. Interstitial flow and its effects in soft tissues. *Annual review of biomedical engineering*, 9:229–256, 2007.

[71] O. Trédan, C. M. Galmarini, K. Patel, and I. F. Tannock. Drug resistance and the solid tumor microenvironment. *Journal of the National Cancer Institute*, 99(19):1441–1454, Oct. 2007.

[72] S. R. Ward and R. L. Lieber. Density and hydration of fresh and fixed human skeletal muscle. *Journal of biomechanics*, 38(11):2317–2320, Nov. 2005.

[73] C. J. Whatcott, H. Han, R. G. Posner, G. Hostetter, and D. D. Von Hoff. Targeting the tumor microenvironment in cancer: why hyaluronidase deserves a second look. *Cancer discovery*, 1(4):291–296, Sept. 2011.

[74] J. A. Wolff, R. W. Malone, P. Williams, W. Chong, G. Acsadi, A. Jani, and P. L. Felgner. Direct gene transfer into mouse muscle in vivo. *Science (New York, N.Y.)*, 247(4949 Pt 1):1465–1468, Mar. 1990.

[75] L. Wu and J. Ding. Effects of porosity and pore size on in vitro degradation of three-dimensional porous poly (D, L-lactide-co-glycolide) scaffolds for tissue engineering. *Journal of Biomedical Materials Research Part A*, 2005.

[76] W. Yao, Y. Li, and G. Ding. Interstitial fluid flow: the mechanical environment of cells and foundation of meridians. *Evidence-based complementary and alternative medicine : eCAM*, 2012:853516, 2012.

[77] A. M. Zöllner, O. J. Abilez, M. Böl, and E. Kuhl. Stretching skeletal muscle: chronic muscle lengthening through sarcomerogenesis. *PloS one*, 7(10):e45661, 2012.

Appendix A Formulation of the model in Ω_0 in the general case

The calculus in the general case gives the final system of equations (77). Recall that matrix B is defined as the inverse of matrix A given by (47). As,

$$(B^{-1})_{i,j} = A_{i,j} = \left(\frac{\partial \Phi(t,\mathbf{X})}{\partial \mathbf{X}}\right)_{i,j} = \delta_{ij} + \frac{\partial u_i}{\partial X_j}(t,\mathbf{X}) = \delta_{ij} + \frac{\partial \overline{u}_i}{\partial \overline{\mathbf{X}}_j}(\overline{t},\overline{\mathbf{X}}), \tag{75}$$

we kept the notation B to refer to $B(\overline{\mathbf{u}})$ in system (77). Note that we equally dropped bars on the dimensionless variables but kept them on the dimensionless parameters. Let us denote

$$J^B_{\text{enz}} = \frac{1}{f}\overline{\boldsymbol{\kappa}}\, B\nabla P - \overline{\mathbf{D}^0_{\text{enz}}} B\nabla f \qquad \text{and} \qquad J^B_{\text{drug}} = \frac{1}{f}\overline{\boldsymbol{\kappa}}\, B\nabla P - \overline{\mathbf{D}^0_{\text{drug}}} B\nabla f. \tag{76}$$

The equivalent system in Ω_0 in dimensionless form reads

$$
\begin{cases}
g_{\mathcal{E}} + g_{\mathcal{C}} + f = 1, & \text{(77a)}\\
\boldsymbol{\nabla} \cdot \left((g_{\mathcal{E}} + g_{\mathcal{C}}) \dfrac{1}{J} B^{-1} \overline{\mathbf{S}_s^E} B^{-T} \right) = \nabla P, & \text{(77b)}\\
(g_{\mathcal{E}} + g_{\mathcal{C}}) \overline{s_0} \dfrac{\partial P}{\partial t} - B\nabla \cdot (\overline{\boldsymbol{\kappa}} B \nabla P) = \alpha Q_{\text{inj}}^{\text{tot}} + \overline{\gamma}(\overline{P_v} - P) - B\nabla \cdot \left(\dfrac{\partial \mathbf{u}}{\partial t} \right) \\
\qquad\qquad + \left(1 - \dfrac{\rho_s^{R,0}}{\rho_f^R} \right) g_{\mathcal{E}} (-\overline{K} h + \overline{a_r} \left(f - f^0 \right)), & \text{(77c)}\\
\dfrac{\partial h}{\partial t} = B\nabla \cdot \left(f \overline{\mathbf{D}_{\text{enz}}^0} B \nabla h + h J_{\text{enz}}^B \right) - \left(\dfrac{\overline{k_{\text{enz}}^d}}{f} + B\nabla \cdot \left(\dfrac{\partial \mathbf{u}}{\partial t} \right) \right) h + \dfrac{\alpha \mathcal{S}_{\text{enz}}}{c_0}, & \text{(77d)}\\
\dfrac{\partial g_{\mathcal{C}}}{\partial t} + g_{\mathcal{C}} \left(\overline{s_0} \dfrac{\partial P}{\partial t} + B \boldsymbol{\nabla} \cdot \left(\dfrac{\partial \mathbf{u}}{\partial t} \right) \right) = 0, & \text{(77e)}\\
\dfrac{\partial g_{\mathcal{E}}}{\partial t} + g_{\mathcal{E}} \left(\overline{s_0} \dfrac{\partial P}{\partial t} + B \boldsymbol{\nabla} \cdot \left(\dfrac{\partial \mathbf{u}}{\partial t} \right) \right) = g_{\mathcal{E}} (-\overline{K} h + \overline{a_r} \left(f - f^0 \right)), & \text{(77f)}\\
\dfrac{\partial c}{\partial t} = B\nabla \cdot \left(f \overline{\mathbf{D}_{\text{drug}}^0} B \nabla c + c J_{\text{drug}}^B \right) - \left(\dfrac{\overline{k_{\text{drug}}^d}}{f} + B\nabla \cdot \left(\dfrac{\partial \mathbf{u}}{\partial t} \right) \right) c + \dfrac{\alpha \mathcal{S}_{\text{drug}}}{c_0}, & \text{(77g)}
\end{cases}
$$

where we get (77a) from Assumption 1, (77b) from Equation (21), (77c) from (15), (77d) from (25), (77g) from (29), (77f) from (13a) and (77e) from (13b), using (51), (52) and (53).

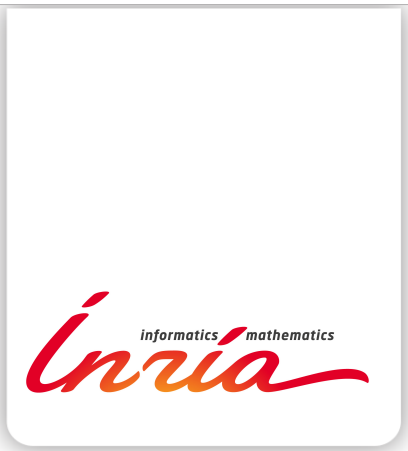

RESEARCH CENTRE
BORDEAUX – SUD-OUEST

200 avenue de la Vieille Tour
33405 Talence Cedex

Publisher
Inria
Domaine de Voluceau - Rocquencourt
BP 105 - 78153 Le Chesnay Cedex
inria.fr

ISSN 0249-6399